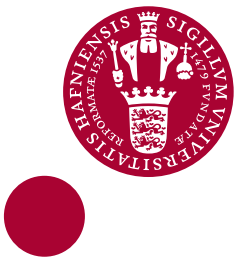

The KDM5 family is required for activation of pro-proliferative cell cycle genes during adipocyte differentiation

Brier, Ann-Sofie B; Loft, Anne; Madsen, Jesper G S; Rosengren, Thomas; Nielsen, Ronni; Schmidt, Søren F; Liu, Zongzhi; Yan, Qin; Gronemeyer, Hinrich; Mandrup, Susanne

Published in:
Nucleic Acids Research

DOI:
10.1093/nar/gkw1156

Publication date:
2017

Document version
Publisher's PDF, also known as Version of record

Published online 28 November 2016

Nucleic Acids Research, 2017, Vol. 45, No. 4 ***1743–1759***
doi: 10.1093/nar/gkw1156

The KDM5 family is required for activation of pro-proliferative cell cycle genes during adipocyte differentiation

Ann-Sofie B. Brier[1,†], Anne Loft[1,†], Jesper G. S. Madsen[1,2], Thomas Rosengren[1], Ronni Nielsen[1], Søren F. Schmidt[1], Zongzhi Liu[3], Qin Yan[3], Hinrich Gronemeyer[4] and Susanne Mandrup[1,*]

[1]Department of Biochemistry and Molecular Biology, University of Southern Denmark, 5230 Odense M, Denmark, [2]The Novo Nordisk Foundation Center for Basic Metabolic Research, University of Copenhagen, 2200 Copenhagen N, Denmark, [3]Department of Pathology, Yale School of Medicine, New Haven, CT, USA and [4]Equipe Labellisée Ligue Contre le Cancer, Department of Functional Genomics and Cancer, Institut de Génétique et de Biologie Moléculaire et Cellulaire, Centre National de la Recherche Scientifique, UMR7104, Institut National de la Santé et de la Recherche Médicale, U964, Université de Strasbourg, Illkirch, France

Received January 22, 2016; Revised November 01, 2016; Editorial Decision November 03, 2016; Accepted November 05, 2016

ABSTRACT

The KDM5 family of histone demethylases removes the H3K4 tri-methylation (H3K4me3) mark frequently found at promoter regions of actively transcribed genes and is therefore generally considered to contribute to corepression. In this study, we show that knockdown (KD) of all expressed members of the KDM5 family in white and brown preadipocytes leads to deregulated gene expression and blocks differentiation to mature adipocytes. KDM5 KD leads to a considerable increase in H3K4me3 at promoter regions; however, these changes in H3K4me3 have a limited effect on gene expression per se. By contrast, genome-wide analyses demonstrate that KDM5A is strongly enriched at KDM5-activated promoters, which generally have high levels of H3K4me3 and are associated with highly expressed genes. We show that KDM5-activated genes include a large set of cell cycle regulators and that the KDM5s are necessary for mitotic clonal expansion in 3T3-L1 cells, indicating that KDM5 KD may interfere with differentiation in part by impairing proliferation. Notably, the demethylase activity of KDM5A is required for activation of at least a subset of pro-proliferative cell cycle genes. In conclusion, the KDM5 family acts as dual modulators of gene expression in preadipocytes and is required for early stage differentiation and activation of pro-proliferative cell cycle genes.

INTRODUCTION

Methylation of histone proteins constitutes important epigenomic marks involved in the dynamic regulation of the genome in response to external cues. Some histone methylation marks are primarily associated with actively transcribed chromatin, whereas other marks are associated with repressed chromatin (1). These marks may be modulated as a consequence of transcriptional activity, but they can also play an active role in modulating transcription. The formation and removal of these marks at histone residues is catalyzed by residue-specific histone methyltransferases and demethylases, respectively. The biological function of these has classically been tightly linked to their histone modifying catalytic activity; however, recent data indicate that both histone methyltransferases and demethylases may also modulate transcription independently of their histone modifying activities (2–5).

The histone lysine demethylases 5 (KDM5) are members of the family of Jumonji C (JmjC) domain-containing histone demethylases and specifically removes dimethyl (me2) and trimethyl (me3) marks from histone 3 lysine 4 (H3K4) (6,7). The KDM5 family is conserved among many species (8), and in humans and other mammals it comprises four KDM5 paralogues, KDM5A, KDM5B, KDM5C, and KDM5D, which are very similar in structure (Supplementary Figure S1A). Unlike KDM5A and KDM5B, KDM5C

*To whom correspondence should be addressed. Susanne Mandrup, Department of Biochemistry and Molecular Biology, University of Southern Denmark, Campusvej 55, 5230 Odense M, Denmark. Tel: +45 6550 2340; Fax: +45 6550 2467; Email: s.mandrup@bmb.sdu.dk
†These authors contributed equally to this work as first authors.
Present addresses: Anne Loft and Søren F. Schmidt, Institute for Diabetes and Cancer, Helmholtz Zentrum München, 85764 Neuherberg, Germany

and KDM5D are sex-chromosome-specific genes located on the X and Y chromosome, respectively (9,10). Multiple studies of KDM5A (11–14) and KDM5B (15–18) have reported an involvement of these in cancer, and some studies of KDM5C (19,20) and KDM5D (9) indicate that this could be a common feature of all KDM5 family members.

Genome-wide mapping of binding sites of KDM5A (21,22), KDM5B (23), and KDM5C (24) have reported preferential binding to promoter regions, and a study of KDM5D binding near the *Engrailed 2* gene (25) likewise demonstrated highest occupancy at the promoter region. More recently, some studies have reported that KDM5 family members may also regulate gene transcription from non-promoter regions, i.e. putative enhancers (24,26–28).

The H3K4me3 mark removed by the KDM5 family is found primarily at active promoter regions (1,29,30), whereas the H3K4me2 mark is found at both active promoters (31) and enhancers (1,32). Both marks are considered activating (1,33), and consequently members of the KDM5 family have classically been regarded as repressors of transcription. Thus, a corepressor role through silencing of gene expression by demethylation of H3K4me3 at promoters of genes has been described in diverse cellular processes such as cell cycle progression and cellular senescence (12,13,17,21,22,34), circadian rhythm (3), and mitochondrial function (21,35). However, a potential coactivating function of the KDM5s has also been suggested by less defined mechanisms such as through the interaction of KDM5A with pRB (36) or nuclear receptors (37), by the ability of KDM5B to prevent spreading of H3K4 methylation into gene bodies (28), and through binding of KDM5C at enhancer regions where it has been suggested to maintain H3K4 mono-methylation levels (38). Furthermore, the KDM5 *Drosophila* ortholog Lid has also been implicated in transcriptional activation through a complex where dMyc masks the demethylase domain (39) through interaction with and inhibition of the deacetylase Rpd3 (40), or by interacting with the transcription factor FOXO and preventing its ability to be recruited to promoters (41). In a recent study of *Drosophila* knockout (KO) flies, Lid was furthermore found to be required for activation of gene expression of a set of mitochondrial genes independently of the demethylase activity but dependent on the PHD domain that recognizes H3K4me2/3 (4). These reports indicate that the KDM5s affect transcriptional activity by several different mechanisms that may be independent of their demethylase activity.

Histone demethylases have been shown to play an important role in cellular differentiation (2). One of the most well studied differentiation processes is adipogenesis, i.e. the development of fibroblast-like preadipocytes to mature, lipid-containing adipocytes. Numerous studies over the past 30 years, in particular studies using the murine 3T3-L1 preadipocyte cell line, have carefully unraveled major transcriptional players in adipogenesis (42,43). Stimulation of adipocyte differentiation with a hormonal cocktail induces a cascade of transcriptional processes that is driven by at least two waves of transcription factors (TFs), the first of which includes CCAAT/enhancer-binding protein β (C/EBPβ) and the glucocorticoid receptor. These factors then induce the expression of the second wave of adipogenic TFs such as C/EBPα and peroxisome proliferator-activated receptor γ (PPARγ), which switches on the adipocyte gene program. A major early event in the differentiation of 3T3-L1 preadipocytes is mitotic clonal expansion, during which the cells undergo approximately two rounds of cell division. This clonal expansion is driven by C/EBPβ (44) and other first wave transcription factors and has been shown to be required for differentiation (45–47). During 3T3-L1 adipogenesis, histone methylation patterns are dramatically changed (48–50). Several histone methyltransferases and histone demethylases have been reported to play a significant role in adipocyte differentiation (51,52). However, so far a role for the KDM5 family in adipocyte differentiation has not been described.

In the present study, we demonstrate that the KDM5 family is required for activation of pro-proliferative cell cycle genes and differentiation of 3T3-L1 as well as brown preadipocytes in response to adipogenic inducers. Using genome-wide approaches, we show that the KDM5s are required for balancing the levels of the activating mark H3K4me3 at promoters in 3T3-L1 cells. Interestingly however, the KDM5s appear to be exerting their main action on adipogenic gene expression as direct coactivators of a subset of promoters including promoters driving pro-proliferative cell cycle genes during adipogenesis.

MATERIALS AND METHODS

Cell culture

3T3-L1 cells were grown in Dulbecco's modified Eagle's medium (DMEM) supplemented with 10% calf serum. Cells were induced to differentiate two days post confluence (designated day 0) in DMEM supplemented with 10% fetal bovine serum (FBS), 1 μM dexamethasone (dex), 0.5 mM 3-isobutyl-1-methylxanthine (MIX), and 1 μg/ml insulin essentially as described previously (53).

Mouse brown preadipocytes immortalized with the SV40 large T antigen were grown in DMEM supplemented with 10% FBS. Cells were induced to differentiate at confluency (designated day 0) in DMEM supplemented with 10% FBS, 0.5 μM dex, 0.5 mM MIX, 20 nM insulin, 1nM T2, and 125 nM indomethacin. From day 2, dex, MIX, and indomethacin were omitted from the differentiation medium.

At indicated time points during differentiation a 0.0025mm^2-counting chamber was used to count the number of cells in control and KD samples. Oil red O staining was performed to evaluate accumulation of lipids in mature adipocytes. Cells were fixed with 3.7% paraformaldehyde for 1 hour and stained for 1 hour with filtered Oil red O solution (0.5 g Oil red O in 100 ml isopropanol) diluted 3:2 in milliQ. Cells were washed in milliQ and microscopy photographs were taken at 450 nm. Immortalized KDM5A-/- mouse embryonic fibroblast (MEFs) with re-introduction of wild-type KDM5A or KDM5A-H483A mutant were described previously (7).

Bromodeoxyuridine (BrdU) assay

A BrdU assay (Millipore) was used to quantify the amount of newly synthesized DNA in control and KD cells in accordance with the manufacturer's instructions. Briefly, cells

were seeded in 96-well NUNC plates in five parallel replicates for each condition and 1:500 BrdU reagent was added to the medium for either 12 h between day 0 and 12 h post-induction of differentiation or for 24 hours between day 1 and day 2 of the differentiation. Following DNA denaturation, the amount of BrdU incorporation was assessed immunochemically as described in the manufacturer's protocol using a spectrophotometer microplate reader at 450 nm.

RNA extraction, cDNA synthesis, and quantitative real-time PCR

RNA extraction, cDNA synthesis, and quantitative real-time PCR were performed as previously described (54). Data were normalized to transcription factor II B (TFIIB) and a two-tailed Student's t-test was used to determine significance. Sequences of real-time PCR primers can be found in Supplementary Table S1.

Western blotting and ECL detection

Whole-cell extracts were prepared in SDS-containing buffer and subjected to western blotting as previously described (54). The following antibodies were used: anti-PPARγ (E-8; sc-7273, Santa Cruz (SC) Biotechnology), anti-C/EBPα (14AA; sc-150, SC Biotechn.), anti-C/EBPβ (C-19; sc-61, SC Biotechn.), anti-KDM5A (ab70892, Abcam), anti-KDM5B (ab50958, Abcam), anti-KDM5C (A301-034A, Bethyl lab.), H3K4me2 (9726, Cell Signaling Techn.), H3K4me3 (8580, Abcam), H3 (2650; Cell Signaling Techn.), anti-rabbit IgG (P0399, DAKO), and anti-mouse IgG (P0447, DAKO), anti-TFIIB (sc-225, SC Biotechn.) was included as a loading control.

Lentiviral production and transduction of 3T3-L1 cells

For KD of KDM5A, -5B, and -5C, shRNA oligos targeting one or more of these factors were cloned into pSicoR PGK puro vectors (Addgene), and lentiviral particles were produced in human embryonic kidney (HEK) 293T cells as described in (55). A control vector containing shRNA targeting luciferase was cloned in parallel. Sequences of shRNA oligos can be found in Supplementary Table S2. Pre-confluent 3T3-L1 and BAT-LgT cells were transduced 4 days before induction of differentiation by incubation for 24 h at 37°C with medium containing lentiviral constructs and 6 μg/ml polybrene (Sigma). After 24 h, the medium was changed to normal growth medium.

Chromatin immunoprecipitation (ChIP)

ChIP experiments were performed in 3T3-L1 preadipocytes (day 0), and in 3T3-L1 cells 4 h and 2 days post-induction of differentiation essentially as previously described (56). For preparation of material for KDM5A and KDM5C ChIP-seq, cross-linking of the chromatin was performed with 2 mM disuccinimidyl glutarate (DSG) (Proteochem) as described previously (57). Chromatin prepared for H3K4me3 ChIP-seq was cross-linked in 1% formaldehyde only. The antibodies used were anti-KDM5A (ab70892, Abcam), anti-KDM5C (A301-034A, Bethyl lab.), and anti-H3K4me3 (8580, Abcam).

RNA-seq preparation and library construction

Total RNA (4 μg) obtained from two independent biological experiments was polyA-selected and subsequently subjected to fragmentation and cDNA-synthesis using the TruSeq RNA Sample Prep kit v2 (Illumina). RNA-seq and ChIP-seq libraries were constructed according to the manufacturer's instructions (Illumina) as described (58) and sequenced on our in-house HiSeq 1500 platform.

Data analysis

Microarray analysis. The microarray data of KDM5A-/- MEFs stably transduced with either empty vector (EV), KDM5A WT or KDM5A-H483A mutant (MT) were used for the analysis. Raw profiling data were normalized with affy::RMA and further processed using the Limma R package (59). A list of differentially expressed genes in cells overexpressing KDM5A WT compared to control (EV) cells were called using a FDR <0.1.

RNA-seq data analysis. Sequencing reads were aligned to the mouse reference genome (version mm9) using Bowtie2 (60). Splice-junction reads were handled by creation of a pseudo-splice genome, similar to the strategy utilized in RSEQTools (61) and aligned using Bowtie2 with standard parameters. Reads were filtered post-alignment for a MAPQ score greater than or equal to 30. The number of exon reads for all RefSeq genes was counted using Subread (62) and differential expression analyses were performed using DESeq2 (FDR <0.05, paired analysis) (63). Clustering of RNA-sequencing data was performed using Mfuzz (64), only including genes with a membership value >0.5 for subsequent analysis. For both microarray and RNA-seq data, functional enrichment analysis was performed with HOMER (65) using pathways related to metabolism from the KEGG database annotation (66,67) and WikiPathways (68).

ChIP-seq data analysis. ChIP-seq data sets were mapped to the mm9 genome with STAR (69) set to not map across splice junctions (–alignIntronMax 1 –outSJfilterIntronMaxVsReadN 0). Tag directories for each ChIP-seq library were generated using HOMER (65), where KDM5A and KDM5C ChIP-seq tag counts were normalized to 10M reads. Since H3K4me3 protein levels are generally higher in KDM5 KD compared with control cells, we used a two-stage normalization strategy to correct for biases in the H3K4me3 libraries and avoid underestimating the global increase in the H3K4me3 levels in the normalization process. First, genome-scale normalization on background reads were done by counting tags in 10 kb windows throughout the genome as described in (70) and normalized using a relative log expression (RLE) method normalization (63). Second, the signal in peaks was normalized for each condition over time, but not across conditions. This two-stage normalization scheme assumes that the background is similar for all conditions (control and KD) and time points and that the signal for a particular condition is constant for most sites over time, but can be different between conditions. Regions enriched for H3K4me3, KDM5A, and KDM5C

were called in each library with HOMER findPeaks using the '-style histone' and '-F 10' settings with all other parameters set at default. For H3K4me3, KDM5A, and KDM5C peak files, overlapping regions were merged into one master region file for each factor/mark. Subsequently, KDM5A and H3K4me3 peaks at each condition were identified as having 10-fold more average normalized tags over two replicates relative to the input control. Due to the lower quality and therefore higher background of the KDM5C profiles, KDM5C peaks were identified as having 4-fold more normalized tags in both KDM5C replicates relative to the input control. For analyses of the H3K4me3 libraries, high confidence promoter proximal regions were identified as being within ±3 kb of transcriptional start site (TSS) and having more than 50 tags/kb in at least one of the conditions resulting in a merged region file consisting of 10,702 H3K4me3 promoter proximal regions. KDM5A and KDM5C promoter proximal binding sites were defined as being within ±1 kb of TSS and distal binding sites between 5 and 50 kb away from TSS. Regions with significantly different levels of H3K4me3 in KD compared to control at each time point (i.e. day 0, 4 h, day 2) were identified using DESeq2 (63) with a fold change cut-off at 1.5-fold averaged over the two replicate experiments and a *P*-adjusted value <0.05. Clustering of the temporal profile of H3K4me3 regions during differentiation was performed with Mfuzz, as described above (64). HOMER was used for counting tags at identified regions, annotating binding sites to RefSeq genes, generating average profiles, and count matrices for heat maps as well as performing motif analyses in KDM5A promoter binding sites. The University of California at Santa Cruz (UCSC) Genome Browser (71) was used for visualization of genome tracks. For analyses of promoter features, we retrieved 2,742 promoters containing TATA boxes from the Eukaryotic Promoter Database (EPDnew) (72). We overlapped these promoter sequences with the respective gene groups and considered a gene as having a TATA box in the promoter if it was found within ±100 bp of the TSS of the RefSeq-annotated gene. We retrieved the position of 16,026 CpG islands from the UCSC genome browser (73) and considered a gene as having a CpG-island promoter when the TSS of the RefSeq-annotated gene overlapped a UCSC CpG island. A group of 17,515 RefSeq-annotated promoters were included as a control.

Statistics. Two-tailed Student's *t*-test was used to determine significance in qPCR analyses. The *P*-value for the difference between data in box plots was computed using Wilcoxon rank sum test. Spearman's correlation coefficient was used to determine the linear correlation between two data sets. In the cluster analysis, 95% confidence interval around the medians was determined by bootstrapping and significance was calculated using a non-parametric Wilcoxon test. The *P*-value between data containing categorical variables was computed using Pearson's Chi-squared test and the two-proportion z-test.

Additional data sets

m5CpG profiles from mature 3T3-L1 adipocytes (day 6 post-induction) (74) was obtained from NCBI Gene Expression Omnibus (GEO) (accession GSE73434).

Data access

The RNA-seq and ChIP-seq data sets generated in this study have been submitted to the GEO (http://www.ncbi.nlm.nih.gov/geo/) under accession number GSE84410. The raw microarray data is deposited in GEO under accession number GSE84309.

RESULTS

KD of the KDM5 family inhibits adipogenesis

In order to identify histone demethylases important for adipocyte differentiation, we constructed a lentiviral short hairpin RNA (shRNA) library to individually KD a large number of histone demethylases in 3T3-L1 preadipocytes (data not shown). Major advantages of the 3T3-L1 model system are that the cells differentiate in a rather synchronous manner in response to a hormonal cocktail, and that differentiation does not require addition of PPARγ agonists for differentiation (75). This is important, since PPARγ agonists are very powerful inducers of adipogenesis and therefore tend to override modest inhibitors of differentiation. Importantly, most of the key adipogenic regulators identified in this system have proven to hold up *in vivo*. The screen identified the KDM5 family among the top hits required for adipogenesis. Of the KDM5 family members only KDM5A, -B, and -C are expressed in 3T3-L1 preadipocytes. These subtypes are expressed at approximately equal levels and none of the family members display major regulation at the mRNA level during adipocyte differentiation (Supplementary Figure S1B).

To further evaluate the role of the KDM5 family members in adipocyte differentiation, we knocked down KDM5A, KDM5B and KDM5C in 3T3-L1 preadipocytes four days prior to induction of differentiation (Figure 1A and B). KD of KDM5B alone did not appear to result in any major effects on the differentiation as indicated by lipid accumulation (Supplementary Figure S1C and D). However, the combined KD of KDM5A and KDM5C, and even more so KD of all three KDM5s, resulted in a marked inhibition of lipid accumulation compared with shLuciferase control cells (Figure 1C and Supplementary Figure S1C and D), thereby indicating redundancy between the KDM5 family members. Accordingly, at day 6 of differentiation the expression levels of adipocyte characteristic genes such as fatty acid binding protein 4 (*Fabp4*), perilipin 1 (*Plin1*), perilipin 2 (*Plin2*), and lipoprotein lipase (*Lpl*) are significantly reduced in the KDM5A/B/C KD (KDM5 KD) cells, while genes characteristic of preadipocytes such as delta-like 1 homolog (Drosophila) (*Dlk1*) and thrombospondin 1 (*Thbs1*) are expressed to higher levels compared with control cells (Figure 1D). Interestingly, KD of the KDM5s does not seem to influence the initial induction of C/EBPβ (Figure 1E and F), which is part of the first wave of transcription factors induced during adipogenesis and required for

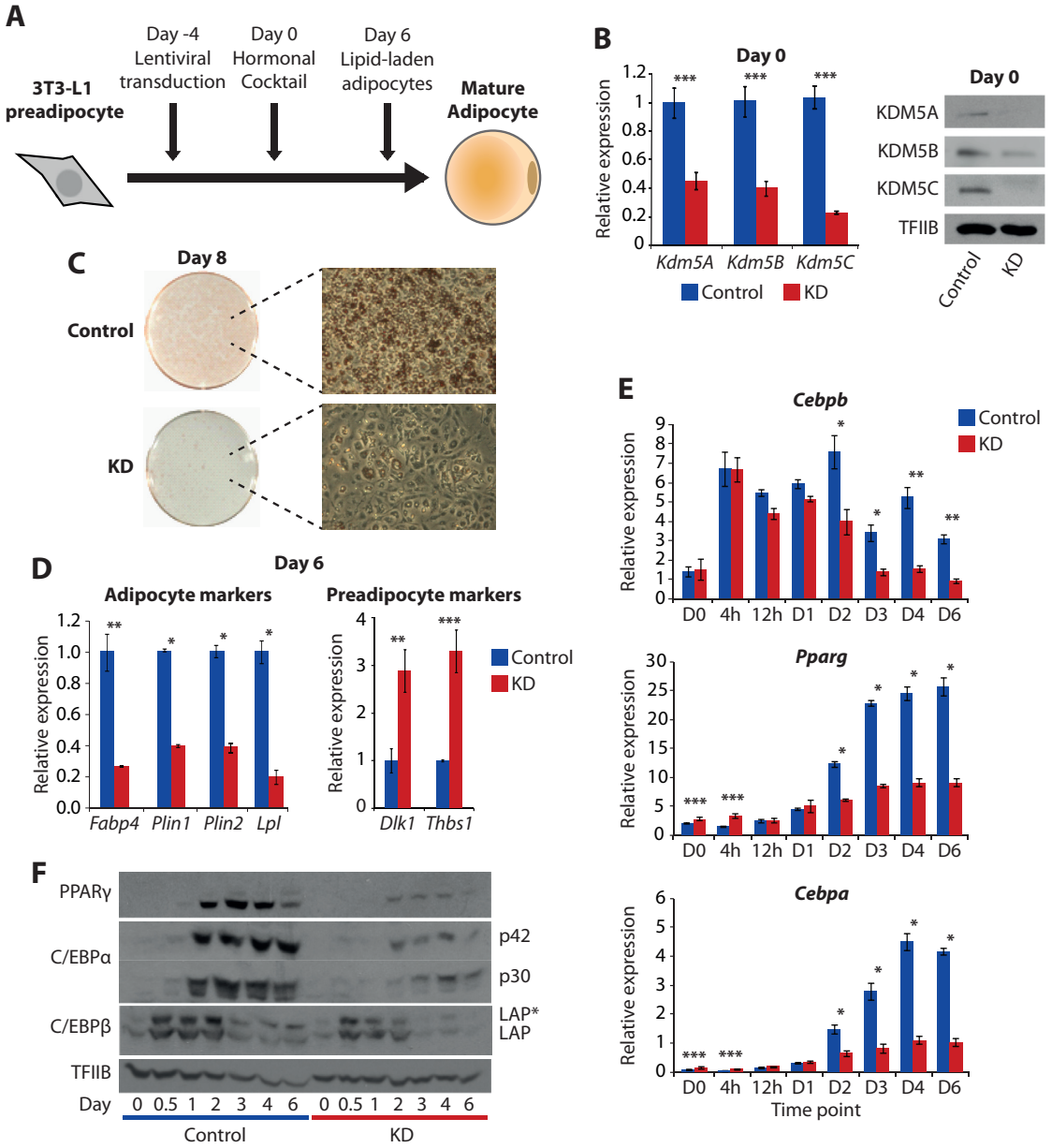

Figure 1. KD of KDM5 family members in 3T3-L1 preadipocytes inhibits adipogenesis. Pre-confluent (day -4) cells were transduced with lentivirus expressing either control luciferase shRNA (control) or shRNA targeting KDM5A, KDM5B, and KDM5C (KD). Cells were induced to differentiate 2 days post confluency (day 0) using a standard differentiation cocktail. (**A**) Schematic representation of the experimental setup. (**B**) mRNA (left) and protein (right) levels of KDM5A, KDM5B, and KDM5C at day 0 in control cells and KDM5 KD cells. (**C**) Representatives of phase contrast micrographs from Oil red O staining performed at day 8 in control and KDM5 KD cells. (**D**) mRNA levels of adipocyte marker genes (left), and preadipocyte marker genes (right) at day 6 in control cells and KDM5 KD cells. mRNA (**E**) and protein (**F**) levels of the key adipocyte transcription factors C/EBPβ, PPARγ, and C/EBPα during the course of adipocyte differentiation in control and KDM5 KD cells. Error bars represent standard deviation (SD), ($n = 3$). *P <0.05, **P <0.01, and ***P <0.005, Student's two-tailed t-test.

mitotic clonal expansion (75). However, induction of the key adipogenic second wave factors, PPARγ and C/EBPα, around day 2 of differentiation is significantly impaired in the KD cells (Figure 1E and F). Importantly, around the same time point at this still early phase in the differentiation process, C/EBPβ levels decrease in KD compared with control cells (Figure 1E and F). Collectively, these data indicate that the KDM5 family is required for activation of the second wave of TFs and for proper progression of 3T3-L1 adipocyte differentiation.

The increase in H3K4me3 promoter levels upon KDM5 KD has limited impact on gene expression

The KDM5 family of histone demethylases is responsible for removing the activating histone mark H3K4me3 primarily located at promoter regions of actively transcribed genes. We therefore hypothesized that the effect on adipocyte dif-

ferentiation by the KDM5 KD was the result of increased levels of H3K4me3 at promoters leading to aberrant activation of genes. Using western blotting we confirmed that KD of the KDM5s leads to a global increase in H3K4me3 that is maintained throughout adipogenesis, whereas it has modest effects on H3K4me2 levels (Figure 2A). To be able to quantify and locate changes in H3K4me3 deposition at the genome-wide level and correlate this with changes in gene expression, we performed H3K4me3 ChIP-seq and RNA-seq in preadipocytes (day 0) and at early time points (4 h and 2 days) during 3T3-L1 differentiation. Importantly, there is a good concordance between the biological replicates for both H3K4me3 ChIP-seq and RNA-seq data sets (Supplementary Figure S2). In total, we identify 10,702 promoters with levels of H3K4me3 significantly above background. In accordance with the total level of H3K4me3 detected by western blot, the average H3K4me3 level at promoters is significantly higher in KDM5 KD compared with control cells (Supplementary Figure S3A). Using a cutoff of Padj$<$0.05, $>$1.5-fold change, we identified 2,145 promoter sites with significantly increased levels of H3K4me3 in KD preadipocytes compared with control cells, whereas only four promoters have reduced H3K4me3 levels (Figure 2B). Similar patterns are observed at 4 h and day 2 of differentiation (Supplementary Figure S3B). Interestingly, evaluation of the correlation between the increase in H3K4me3 at promoters in KD relative to control cells and the increase in gene expression shows that there is only a weak correlation at all time points (Figure 2C, Supplementary Figure S2C). Accordingly, for the genes that are associated with increased H3K4me3 signal in the KD cells there is a marginal average increase in gene expression relative to control cells, which is a remarkably small effect given the considerable increase in H3K4me3 levels (Figure 2D).

The majority of promoter sites gaining H3K4me3 signal upon KDM5 KD are also marked by H3K4me3 in the control cells (Figure 2E), and we therefore speculated that the degree to which promoters are already marked by H3K4me3 could influence the transcriptional impact of an increase in H3K4me3. To evaluate this possibility, we grouped the 2145 preadipocyte promoters with gain in H3K4me3 upon KDM5 KD into quartiles based on H3K4me3 signal in control cells, with quartile 1 having the lowest H3K4me3 signal (Figure 2E). The largest fold increase in H3K4me3 in KD compared with control cells is observed in quartile 1 (Figure 2F), and the average fold increase in expression of associated genes is also slightly higher in quartile 1 (Figure 2G). However, genes associated with quartile 1 promoters are generally expressed at low levels (Supplementary Figure S3D), and the correlation between fold increases in H3K4me3 level and fold changes in gene expression is weak for all of the quartiles (Supplementary Figure S3E). Examples of ChIP-seq profiles of H3K4me3 promoter sites of the four quartiles as well as the gene expression of the associated genes are presented in Figure 2H. These analyses demonstrate a surprising degree of disconnection between the increased promoter-associated H3K4me3 signal and induction of transcription by KDM5 KD in 3T3-L1 cells.

KDM5 KD leads to an increase in H3K4me3 at dynamically regulated promoters

The above analyses investigated the relationship between the increase in H3K4me3 at promoters and gene expression in preadipocytes at early time points of the differentiation process. In order to evaluate whether KDM5 KD disrupts the dynamic changes in the level of H3K4me3 at a subset of promoters thereby resulting in aberrant gene expression of these promoters, we performed a temporal profile cluster analysis of the H3K4me3 mark at promoters using Mfuzz (64). First, we identified all promoter sites that exhibited differential levels of H3K4me3 in control versus KD cells at one or more of the analyzed time points (i.e. day 0, 4 h and/or day 2). Second, we clustered these promoters according to their changes in H3K4me3 levels during the early time points of the differentiation (Figure 3A). In accordance with the global increase in H3K4me3 levels in the KD cells, all identified clusters have significantly higher levels of H3K4me3 in KD compared with control cells (Figure 3B). However, as previously observed in the analysis of all promoters (Figure 2D), the substantial increase in H3K4me3 levels upon KD at these dynamically regulated promoter regions appears to have very little effect on the expression of the associated genes (Figure 3C). Collectively, we find little evidence indicating that the considerable gain in promoter H3K4me3 levels resulting from KD of the KDM5s is causally related to the changes in gene expression.

Increased gene expression correlates with increased H3K4me3 levels

The above analyses indicate that an increase in promoter proximal H3K4me3 *per se* is not a strong inducer of gene expression. We therefore addressed the reverse question, i.e. whether an increase in transcriptional activity upon KDM5 KD is reflected in an increase in H3K4me3 at the corresponding promoters. To investigate this, we identified a set of genes that were differentially expressed (Padj $<$0.05) between KD and control cells at day 0 (Figure 4A), or at 4 h and 2 days post-induction of differentiation (Supplementary Figure S4A). A substantial number of dysregulated genes are detected at all time points, with the largest number of dysregulated genes found at day 2 (i.e. 798 regulated genes at day 0; 825 genes at 4 h; and 1,987 genes at day 2) (Figure 4A and Supplementary Figure S4A). In line with this, clustering analyses based on temporal gene expression pattern (day 0 to day 2) in control cells (Supplementary Figure S4B) reveal that the first wave of gene regulation initiated by the adipogenic stimuli at day 0 is not greatly affected by the reduced KDM5 levels, whereas subsequent gene regulation at day 2 is dysregulated upon KDM5 KD (Supplementary Figure S4C). Thus, KDM5 KD leads to a profound dysregulation of gene expression at day 2 of adipocyte differentiation.

Notably, a similar number of genes are upregulated and downregulated in response to KDM5 KD at all time points, supporting the notion that the KDM5s have both activating and repressive effects on gene expression as reported in previous studies (28,36–38). For genes activated by the KDM5 KD, a strong correlation is observed between the

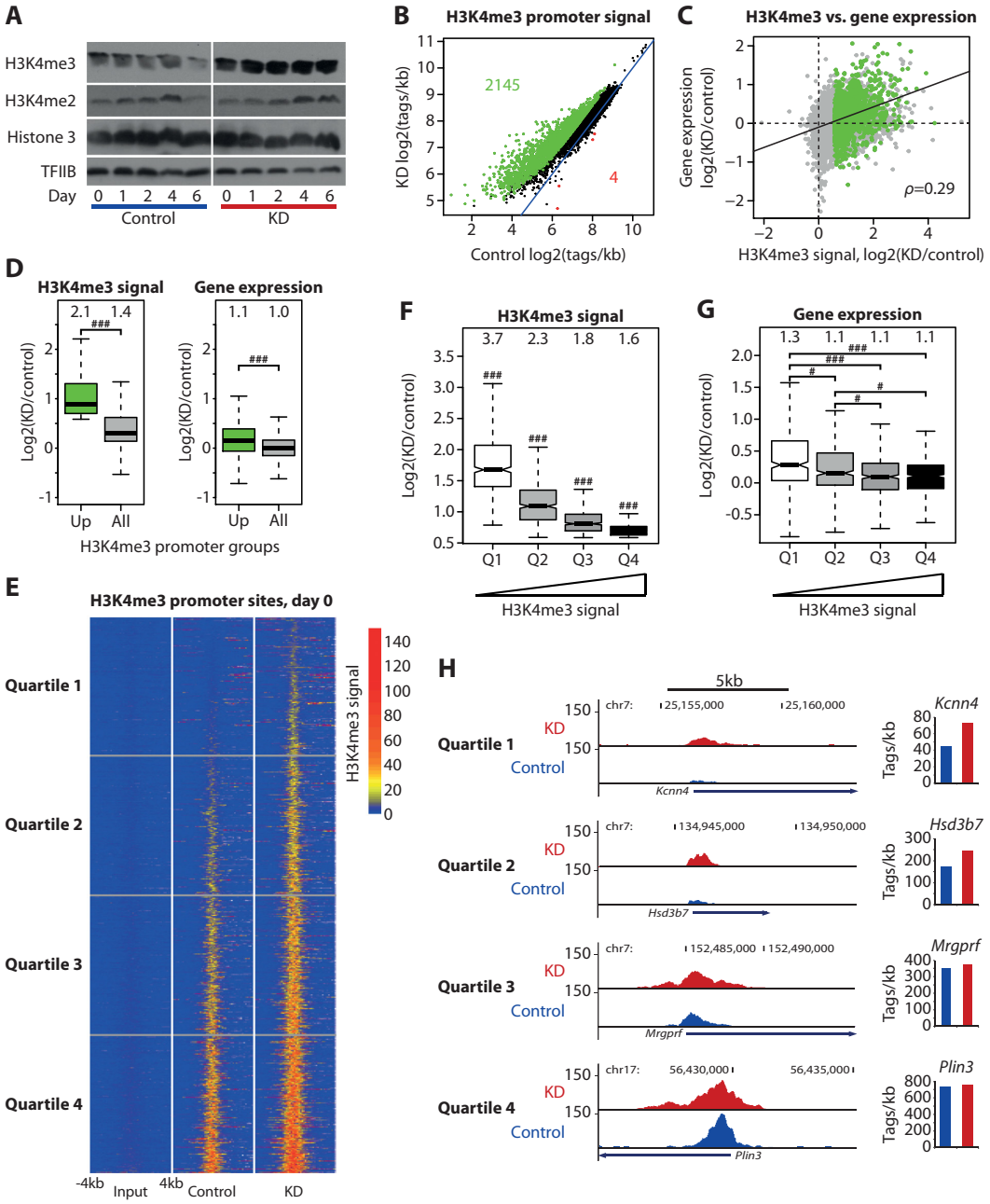

Figure 2. H3K4me3 levels are globally increased at promoters upon KDM5 KD. (**A**). Western blot showing levels of total H3K4me3 and H3K4me2 protein during the course of differentiation in control and KDM5 KD cells with histone H3 and TFIIB included as controls. (**B**) Scatter plot showing the normalized log2 H3K4me3 promoter signal (as tags per kb) (i.e. sites located within -3 kb to +3 kb of the transcription start site (TSS)) in control and KDM5 KD cells at day 0. H3K4me3 sites with significantly higher tag count (Padj<0.05, min 1.5-fold change) in KDM5 KD relative to control (green) or control relative to KD (red) cells are shown. (**C**) Scatter plot showing the log2 fold change in H3K4me3 promoter signal related to the log2 fold change in expression of the nearest genes in KDM5 KD relative to control cells at day 0 at all identified H3K4me3 sites of an expressed gene. H3K4me3 promoter sites with significantly higher tag count (Padj<0.05, min 1.5-fold change) upon KDM5 KD are shown. There are no H3K4me3 promoter sites with significantly lower tag count in KD relative to control cells of expressed genes. 'ρ' indicates Spearman's correlation coefficient and the black line shows the linear regression between plotted values (green) of the H3K4me3 sites with significantly higher tag count in KD cells. (**D**) Box plots showing log2 fold change in H3K4me3 promoter signal (left) and gene expression (right) in KD relative to control cells at day 0 promoter sites of expressed genes that significantly gain H3K4me3 signal (green) or at all H3K4me3 promoter sites (gray). (**E**) H3K4me3 promoter sites were divided into four quartiles (Q1–Q4) based upon H3K4me3 signal in day 0 control cells with Q1 having the weakest signal. Heat map showing input signal in control cells (left panel) and H3K4me3 signal in control (middle panel) and KDM5 KD cells (right panel) at day 0 in a ±4-kb window around H3K4me3 promoter sites that significantly gain H3K4me3 upon KDM5 KD. (**F**) Box plot showing for day 0 the log2 fold change in H3K4me3 promoter signal in KDM5 KD relative to control cells in the four quartiles (Q1–Q4) described in E. (**G**) Box plot showing for day 0 the log2 fold change in gene expression in KDM5 KD relative to control cells in the four quartiles (Q1–Q4) described in E. (**H**) ChIP-seq profiles of H3K4me3 at representative sites from the four quartiles described in E at the *Kcnn4* (Q1), *Hsd3b7* (Q2), *Mrgprf* (Q3), and *Plin3* (Q4) loci (left). Gene expression signal (as tags per kb) of the associated genes in control (blue) and KDM5 KD (red) cells at day 0 (right). D, F and G: *P*-value: # $P < 0.05$, ## $P < 2.2e\text{-}8$, and ### $P < 2.2e\text{-}16$, Wilcoxon rank sum test as indicated or F) between individual quartiles. Fold change of KD relative to control is included above each box.

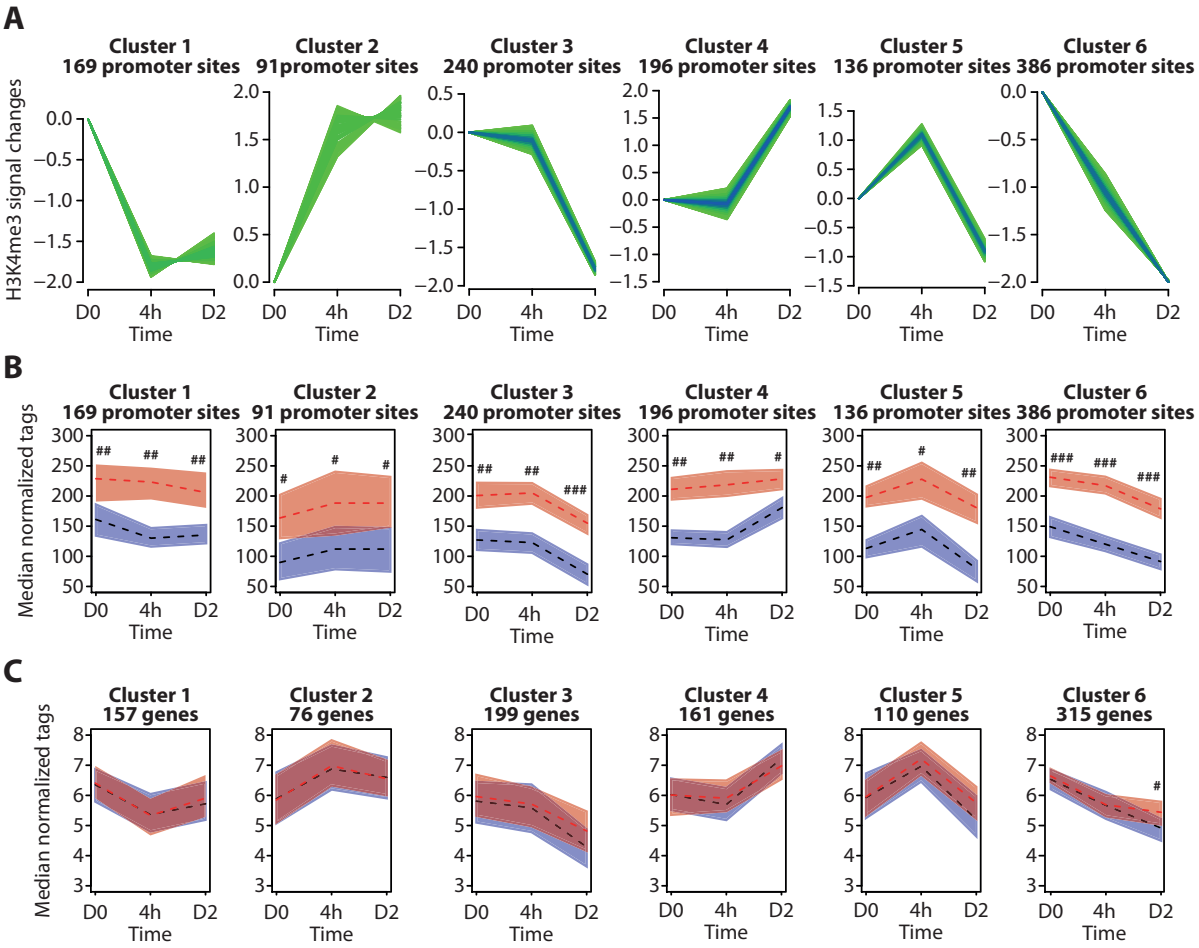

Figure 3. Cluster analysis of temporal H3K4me3 occupancy at promoter sites. (**A**) All promoter sites with differential levels of H3K4me3 in control relative to KDM5 KD cells at one or more of the analyzed time points were clustered based on the temporal profile of H3K4me3 during the early stage of adipocyte differentiation (day 0 to 2) in control cells. (**B**) H3K4me3 promoter signal in the six clusters shown in A in control (blue) and KDM5 KD (red) cells at day 0. The colored region illustrates the 95% confidence interval around the median (dashed line) as determined by bootstrapping. (**C**) Expression signal based on RNA-seq of genes assigned to the promoters from the six different clusters shown in A in control (blue) and KDM5 KD (red) cells at day 0. The colored region is the 95% confidence interval around the median (dashed line) as determined by bootstrapping. The number of genes in C differs from the number of promoter sites in A-B due to a subset of the cluster promoter sites being associated with genes not expressed at detectable levels in 3T3-L1 cells, which were therefore excluded from the analysis. B and C: *P*-value: # $P < 0.05$, ## $P <$ 2.2e-8, and ### $P <$ 2.2e-16, control compared with KDM5 KD, Wilcoxon rank sum test.

increase in gene expression and the increase in H3K4me3 at the promoter (Figure 4B and Supplementary Figure S4D). In line with this, the average gain in H3K4me3 at promoters of genes that are upregulated upon KDM5 KD is significantly higher than the gain in H3K4me3 at promoters of downregulated and all analyzed genes (Figure 4C, right). Notably, genes downregulated upon KDM5 KD do not lose H3K4me3 signal compared with control cells (Figure 4C, right), consistent with the notion that the H3K4me3 mark is not a main determinant of gene expression. Examples of ChIP-seq profiles of H3K4me3 promoter sites and the expression of associated upregulated and downregulated genes are shown in Figure 4D. Taken together, these results indicate that rather than promoting gene expression, the H3K4me3 mark is deposited at promoter regions mainly as a result of active transcription.

KDM5A binding is strongest near KDM5-activated genes

To explore the mechanisms by which the KDM5s are involved in gene regulation during the early stages of 3T3-L1 adipogenesis, we performed KDM5A ChIP-seq in replicates in 3T3-L1 cells at different time points (day 0, 4 h and day 2) of the differentiation. As previously shown (21,22,76), a large proportion of KDM5A binding sites (22.0%) are located in the promoter region (TSS ± 1 kb) (Supplementary Figure S5A), and these correlate very strongly between replicates (Supplementary Figure S5B). Furthermore, KDM5A promoter binding sites display much higher binding intensity than other genomic regions (Supplementary Figure S5C). A comparable binding pattern is observed for KDM5C (Supplementary Figure S5A and S5C), and there is strong correlation between the binding strength of KDM5A and KDM5C at their target promoters (Supplementary Figure S5D), thereby indicating

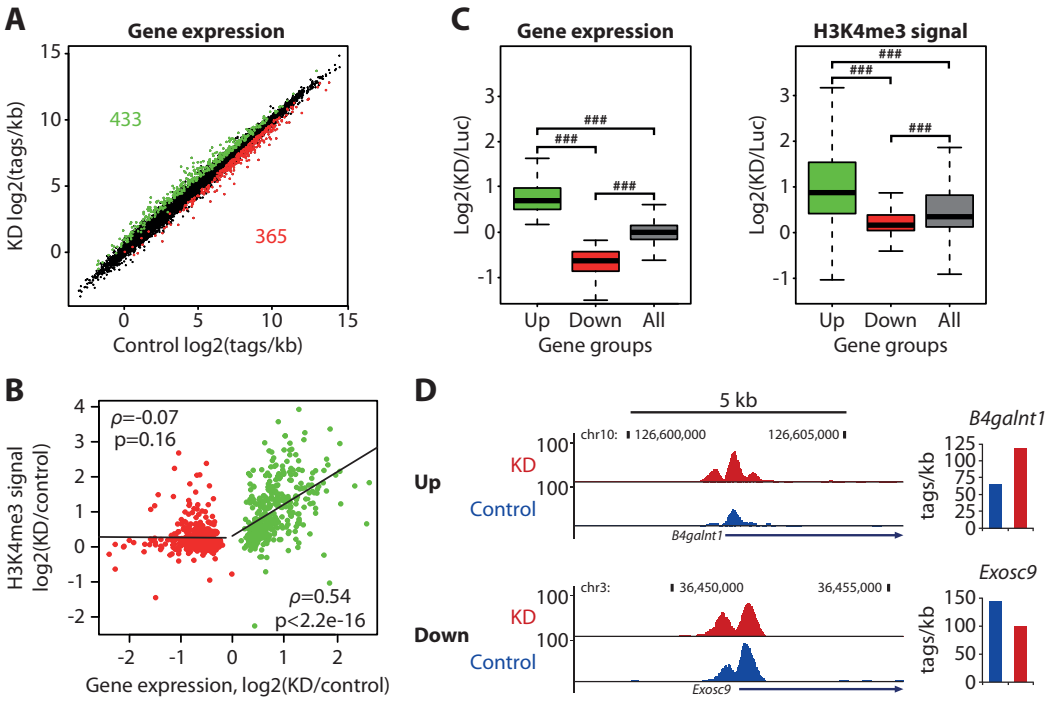

Figure 4. Correlation between gene expression and H3K4me3 signal. (**A**) Scatter plot showing the normalized log2 gene expression signal (as tags per kb) in KDM5 KD relative to control cells at day 0. Genes significantly (Padj <0.05) increased (green) or reduced (red) upon KDM5 KD are highlighted. (**B**) Scatter plot showing the log2 fold change in gene expression signal and the log2 fold change in the associated H3K4me3 promoter signal in KDM5 KD relative to control cells at day 0 at genes that are repressed (red) or induced (green) by KDM5 KD. 'ρ' indicates Spearman's correlation coefficient and the black line shows the linear regression between plotted values. The *P*-value of the Spearman's correlation is indicated. (**C**) Box plot showing the log2 fold change in gene expression signal (left) and the log2 fold change of the associated H3K4me3 promoter signal (right) in KDM5 KD relative to control cells at day 0 at all identified genes (grey), as well as genes that are repressed (red) or induced (green) by KDM5 KD. *P*-value: ### P <2.2e-16, Wilcoxon rank sum test. (**D**) ChIP-seq profiles of H3K4me3 at the *B4galnt1* and *Exosc9* loci and gene expression signal (as tags per kb) (right) in control (blue) and KDM5 KD (red) cells at day 0.

that these two factors display a similar mode of binding in 3T3-L1 cells.

Interestingly, genes with strong promoter binding of KDM5A in preadipocytes tend to be induced and gain H3K4me3 during differentiation (Figure 5A and B, Supplementary Figure S5E), and this gene induction is impaired in the KDM5 KD cells (Figure 5C). This indicates that high KDM5A promoter binding at day 0 primes promoters for activation during early adipogenesis. In contrast, genes with low KDM5A binding in preadipocytes are predominantly repressed during differentiation (Figure 5B), and this repression is KDM5-dependent (Figure 5C). Thus, KDM5A is associated with both induced and repressed promoters during 3T3-L1 adipogenesis; however, promoters marked with low KDM5A binding in preadipocytes are generally repressed in a KDM5-dependent manner during differentiation, whereas promoters with high KDM5A binding are generally activated in a KDM5-dependent manner during differentiation.

To further explore the regulatory role of KDM5 in adipocyte differentiation, we defined a set of KDM5-activated (i.e. bound by KDM5A and downregulated by KDM5 KD) and KDM5-repressed (i.e. bound by KDM5A and upregulated by KDM5 KD) genes. KDM5A binding is significantly stronger at the promoter of these regulated genes compared to regions distal to these genes (Figure 5D). Furthermore, only minor differences in KDM5A binding near KDM5-activated and repressed genes are observed at these distal regions, supporting the notion that KDM5A mainly exerts its effect through the promoter. In accordance with the analyses above, KDM5A binds significantly less to promoters of KDM5-repressed genes compared with KDM5-activated promoters and promoters of all KDM5A target genes (Figure 5D), and these KDM5-repressed genes are expressed at a lower level and have lower levels of H3K4me3 at their promoters (Supplementary Figure S5F and G). These analyses further indicate that KDM5A functions as a repressor at some promoters, which are generally low occupancy sites, whereas it acts as an activator of a subset of high KDM5A occupancy promoters. Similar promoter-enriched binding to KDM5-activated genes is observed for KDM5C thereby further supporting a similar mode of action for KDM5A and KDM5C in 3T3-L1 cells (Supplementary Figure S5H).

Further characterization of KDM5-activated and KDM5-repressed promoters at day 2 revealed that KDM5-activated promoters on average are less associated with a TATA box and are more associated with CpG islands (Figure 5E). Furthermore, comparison with DNA methylation profiles from a previous study (74) showed that KDM5-activated promoters generally are depleted of m5CpG signal in 3T3-L1 adipocytes compared to KDM5-repressed and all target sites (Figure 5F). Interestingly, motif analyses revealed that the E2F7 motif is specifically enriched at

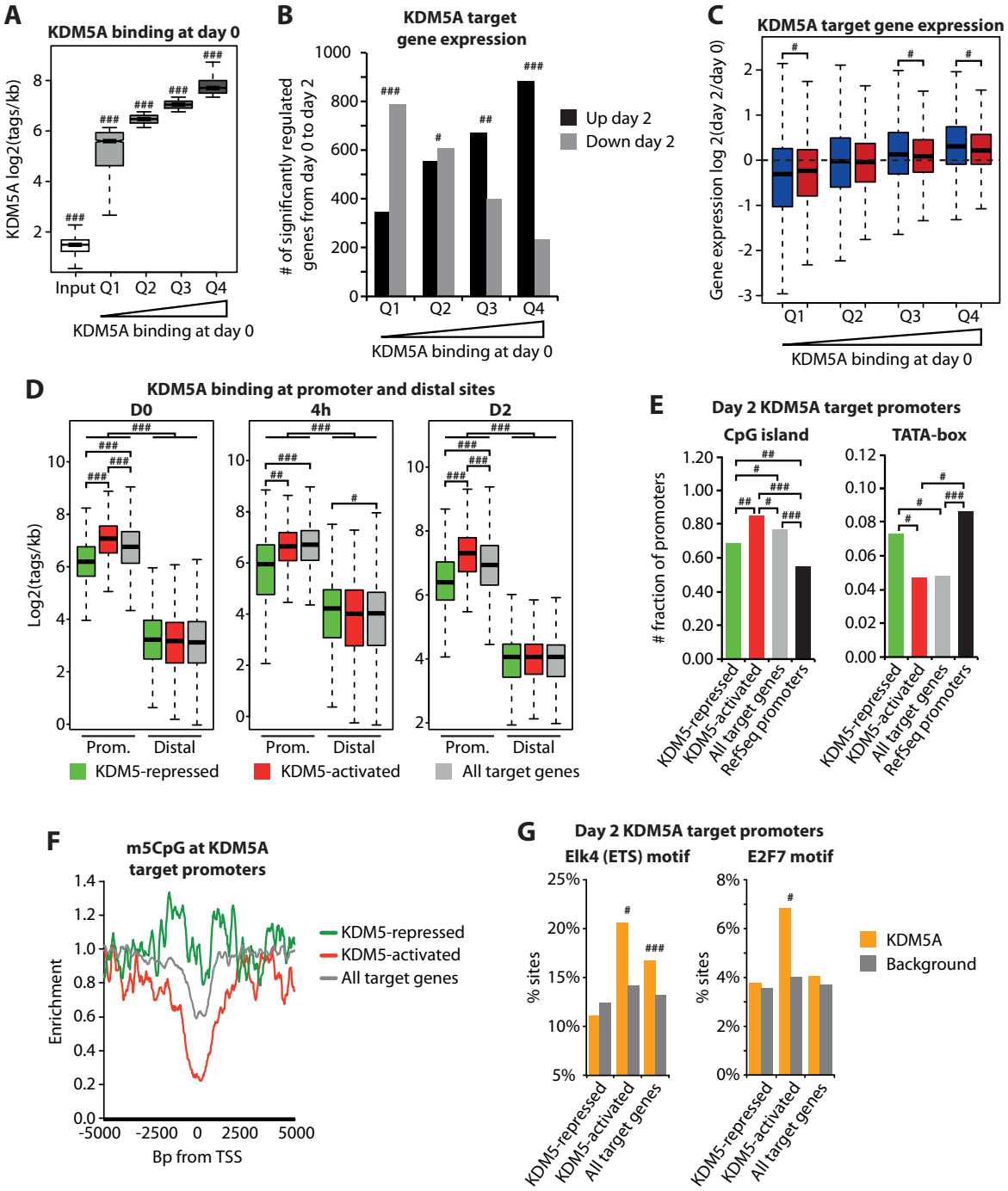

Figure 5. KDM5A binds strongly at promoters of KDM5-activated genes. (**A**) KDM5A promoter sites were divided into four quartiles (Q1-Q4) based on KDM5A signal in 3T3-L1 preadipocytes with Q1 having the weakest signal. (**B**) Number of genes that are significantly induced (black) or repressed (gray) from day 0 to day 2 during differentiation for genes with KDM5A promoter sites in different quartiles (Q1–Q4, defined in A) in control cells. *P*-value: # $P < 0.05$, *P*-value: ## $P < 2.2e\text{-}8$ and ### $P < 2.2e\text{-}16$. Two proportion z-test between induced and repressed genes in each quartile. (**C**) Box plot showing log2 fold change in gene expression signal (as tags per kb) from day 0 to day 2 of differentiation for genes with KDM5A promoter sites in different quartiles (Q1–Q4) in control (blue) and KDM5 KD (red) cells. **D**. Box plot showing log2 normalized KDM5A signal (as tags per kb) in promoter sites (±1 kb from TSS) and distal sites (5–50 kb from TSS) of KDM5-repressed (green), KDM5-activated (red), and all KDM5 target (gray) genes at day 0 (left), 4 h (middle) and day 2 (right) post induction of 3T3-L1 differentiation. (**E**) Fraction of promoter sites for each indicated group of KDM5A-associated day 2 promoters and annotated RefSeq promoters that harbor a CpG island (left) or TATA-box (right). *P*-value: # $P < 0.05$, ## $P < 2.2e\text{-}8$, and ### $P < 2.2e\text{-}16$, Pearson's Chi-squared test. (**F**) Aggregate plot showing the average m5CpG signal (as tags per bp per peak) at day 6 post-induction of 3T3-L1 differentiation in KDM5A day 2 target promoters of KDM5-repressed (green), KDM5-activated (red), and all KDM5 target (gray) genes. (**G**) The percentage of KDM5A day 2 promoter sites (orange) or matched genomic background sequences (gray) with the indicated motifs near KDM5-repressed, KDM5-activated, and all KDM5 target genes. # FDR<0.05 and ### FDR<2.2e-16 between KDM5A promoter groups and background. A, C and D: *P*-value: # $P < 0.05$, ## $P < 2.2e\text{-}8$, and ### $P < 2.2e\text{-}16$, Wilcoxon rank sum test, as indicated or A) between individual quartiles and D) between all groups in promoter and distal regions.

KDM5-activated promoters at day 2, whereas the ETS motif is enriched at KDM5-activated promoters and a control group of all KDM5A-occupied promoters (Figure 5G, Supplementary Table S3), suggesting that members of the KDM5 family and E2F cooperate in the activation of these genes. Taken together these results indicate that the ability of KDM5 to repress or activate promoters may depend on the promoter context.

The KDM5s are required for activation of cell cycle genes and proliferation

To characterize the KDM5 target genes that are dysregulated on day 2 in the KDM5 KD cells, we performed functional enrichment analyses using KEGG and WikiPathways on KDM5-activated, -repressed, and unchanged target genes in day 2 KD cells compared with control. Interestingly, among the top five most significantly enriched pathways of the KDM5-activated target genes are multiple cell cycle-related terms in both the KEGG and WikiPathways analyses (Figure 6A, Supplementary Figure S6A). Genes in this group include cell cycle genes that are involved in stimulation of progression through the cell cycle such as cell division cycle 6 (*Cdc6*) and *Cdc20* (Figure 6B), as well as genes encoding important cell cycle regulators such as E2F transcription factor 1 and 2 (*E2f1* and *E2f2*) (Supplementary Figure S6B). These genes display transient expression profiles that peak around day 2 during differentiation in control cells (Figure 6B), which is consistent with mitotic clonal expansion during the early stage of 3T3-L1 differentiation (45–47). Notably, KDM5 KD impairs the induction of cell cycle genes normally upregulated during early differentiation (Figure 6C, Supplementary Figure S6B), whereas KDM5 KD does not significantly affect cell cycle genes that are repressed or unchanged between day 0 and day 2 (Supplementary Figure S6C). Importantly, and in accordance with other KDM5-activated genes in the above analysis (Figure 5D), the KDM5-activated cell cycle genes also display enrichment of KDM5A and KDM5C binding (Figure 6D-E and Supplementary Figure S6D). Upon KDM5 KD, binding of KDM5A as well as KDM5C to the promoters of a subset of pro-proliferative cell cycle genes is significantly reduced (Figure 6F), indicating that both KDM5 family members play a direct role in the induction of these pro-proliferative cell cycle genes. Collectively, these results show that KDM5 KD prevents the full induction of the cell cycle gene program in response to the adipogenic cocktail and indicates that KDM5 family members directly coactivate these genes. Consistent with a role of KDM5 in activation of cell cycle genes, mitotic clonal expansion between day 1 and day 3 of differentiation (Figure 7A) as well as DNA synthesis (Figure 7B) is significantly impaired in KDM5 KD cells compared with control. Notably, KD of KDM5 at day 2 of the differentiation, i.e. after activation of the second wave of major adipogenic transcription factors and after the post-confluent mitoses, does not interfere with adipogenesis (Supplementary Figure S6E-H). Collectively, these results shows that KD of KDM5 interferes with early stage 3T3-L1 adipogenesis, and indicates that it does so at least in part by interfering with activation of cell cycle genes.

To investigate whether KDM5 plays a similar role in the differentiation of other adipocyte model systems, we knocked KDM5 down in BAT-LgT cells, which is a brown preadipocyte cell line immortalized by SV40 large-T antigen (Supplementary Figure S7A). Interestingly and consistent with the results from 3T3-L1 preadipocytes, KDM5 KD in brown preadipocytes also affects the expression of a subset of cell cycle genes (Supplementary Figure S7B) and results in impaired proliferation during differentiation (Figure 7C). Furthermore, KDM5 KD results in reduction in lipid accumulation (Figure 7D and Supplementary Figure S7C) as well as expression of adipocyte marker genes and UCP1 (Figure 7E). Taken together, the KDM5 family is important for post-confluent proliferation and adipogenesis of immortalized brown preadipocytes as well as 3T3-L1 white preadipocytes, suggesting that these are general effects of KDM5 on ex vivo adipocyte differentiation.

Both gene activation and repression is dependent on KDM5A enzymatic activity

Our results indicate that the KDM5s primarily promote adipogenesis by coactivation of specific promoters including promoters of cell cycle genes, whereas the general effect on reducing H3K4me3 at promoters seems to be less important. To investigate whether the demethylase enzymatic activity of the KDM5s is required for the regulation of cell cycle genes, we used microarray data from KDM5A KO mouse embryonic fibroblasts (MEFs) stably expressing either wild type or an enzymatically inactive mutant of KDM5A. Similar to the results from differentiating 3T3-L1 adipocytes, functional enrichment analyses revealed that gene groups related to the cell cycle and cancer pathways are significantly enriched among the KDM5A-activated target genes in KDM5A KO MEFs (Supplementary Figure S8). The major fraction of these KDM5A-activated cell cycle genes have previously been reported to be pro-proliferative and/or have been shown to be overexpressed in various cancer forms (77–87). Interestingly, we find that the enzymatic activity is required for both activation and repression of genes by KDM5A (Figure 8A). Importantly, with the exception of the proto-oncogenes *Mdm2* and *Ccnd1*, there is a requirement of the demethylase activity for the activation of pro-proliferative cell cycle genes by KDM5A, suggesting that the enzymatic activity of KDM5A is required for the ability to induce the majority of KDM5A-activated cell cycle genes in fibroblasts (Figure 8B and C).

DISCUSSION

In this study, we demonstrate that KD of the KDM5 family impairs proliferation and differentiation in white and brown preadipocytes. We show that KD of the KDM5 histone demethylases in 3T3-L1 preadipocytes results in a global increase in H3K4me3 levels at promoters but that this has little impact on gene expression *per se*. In contrast, our data indicate that KDM5 can act as an activator of a subset of cell cycle genes, and that KD of KDM5 abrogates the induction of these genes in response to the adipogenic cocktail (Figure 8D).

Our approach to simultaneously KD all expressed KDM5 family members, i.e. KDM5A, KDM5B and

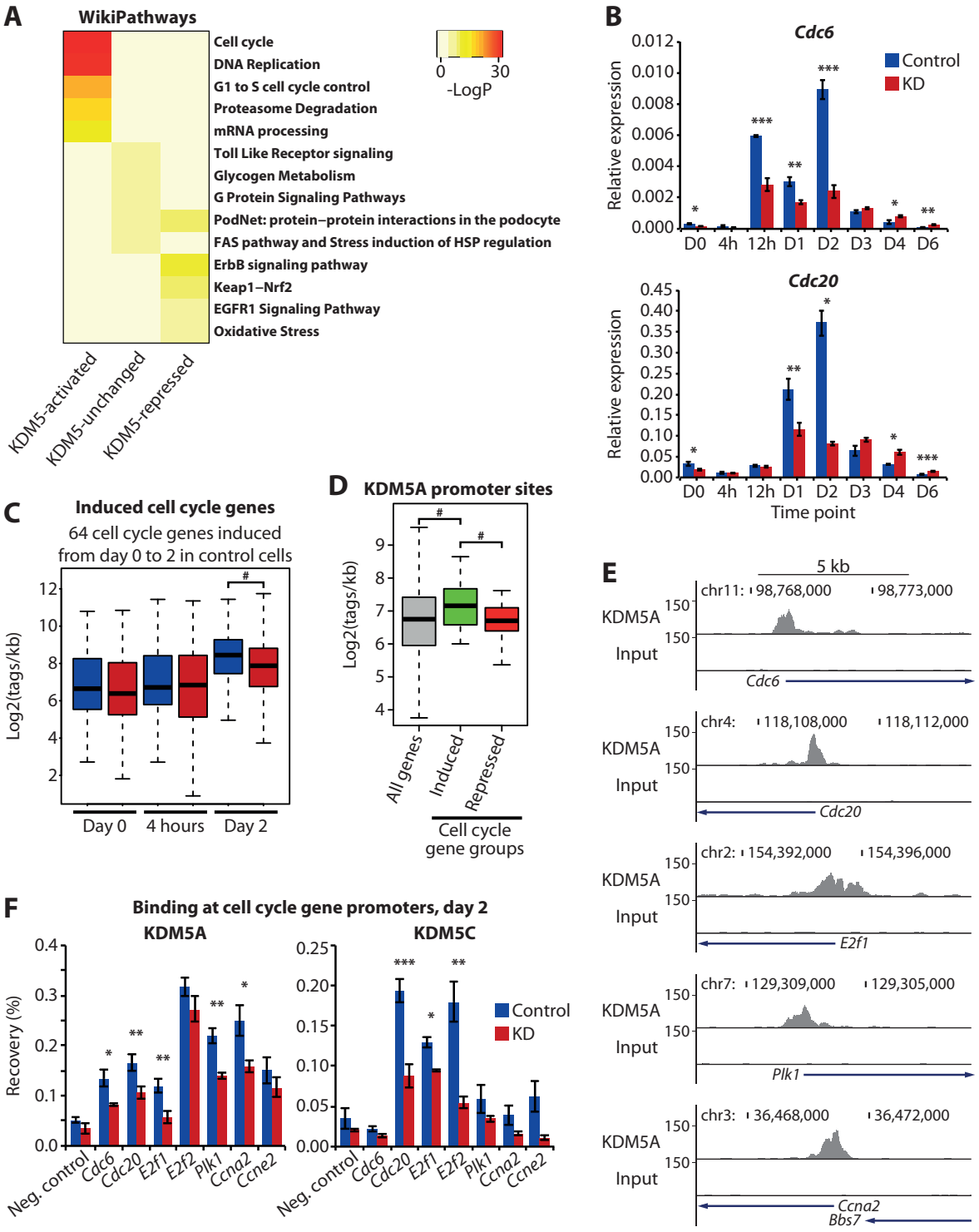

Figure 6. Cell cycle genes are dysregulated in KDM5 KD cells. (**A**) KDM5-repressed genes, KDM5-activated genes, and genes with KDM5A binding in their promoter but unchanged by KD were subjected to functional enrichment analyses. The heat map shows the enrichment (reported as -LogP) for the top 5 WikiPathways in each category. (**B**) mRNA levels of *Cdc6* (top) and *Cdc20* (bottom) during the course of adipocyte differentiation in control (blue) and KDM5 KD (red) cells. Error bars represent SD ($n = 3$). *P*-value: $*P < 0.05$, $**P < 0.01$, and $***P < 0.005$, control compared with KDM5 KD, Student's two-tailed *t*-test. (**C**) Box plots illustrating log2 normalized gene signal (as tags per kb) during differentiation from day 0 to day 2 of induced cell cycle genes from the KEGG database annotation in control (blue) and KDM5 KD (red) cells. (**D**) Box plot showing log2 normalized KDM5A signal at day 2 (as tags per kb) in the KDM5A-occupied promoters of all analyzed genes (gray), as well as cell cycle genes from the KEGG database annotation that are either induced (green) or repressed (red) from day 0 to day 2 of differentiation. (**E**) ChIP-seq profiles of KDM5A at the *Cdc6*, *Cdc20, E2f1, Plk1, and Ccna2* loci at day 2. C and D: *P*-value: # $P < 0.05$, Wilcoxon rank sum test as indicated. (**F**) ChIP-qPCR of KDM5A (left) and KDM5C (right) binding at promoters of selected pro-proliferative genes in control (blue) and KDM5 KD (red) cells presented as percent recovery of input. *P*-value: $*P < 0.05$, $**P < 0.01$, and $***P < 0.005$, positive targets versus negative control (neg. control) as well as control versus KDM5 KD, Student's two-tailed *t*-test.

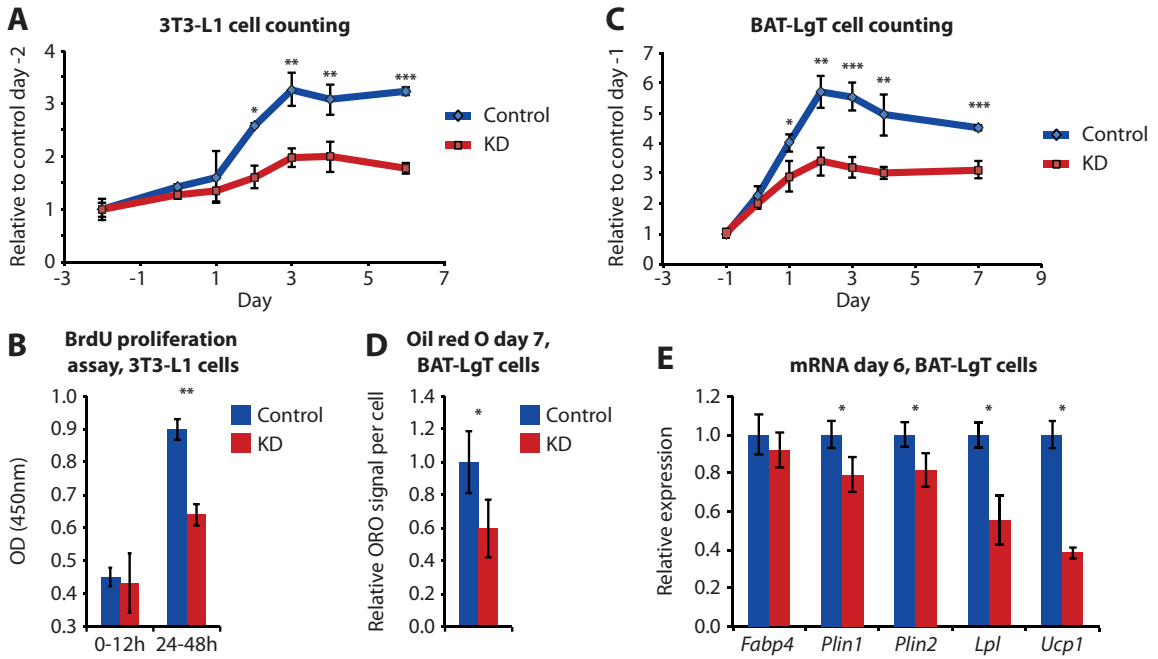

Figure 7. KDM5 KD impairs proliferation in both 3T3-L1 and BAT-LgT differentiating cells. (**A**) Cell counting at the indicated time points during differentiation in control (blue) and KDM5 KD (red) 3T3-L1 cells. The data is presented as a mean of three independent biological replicates and error bars represent SD ($n = 3$). (**B**) BrdU assay performed in 3T3-L1 cells between time of induction of differentiation and 12 h later (0–12 h) and day 1 to 2 after induction of differentiation (24–48 h). Error bars represent SD ($n = 5$), and the data is representative of two independent biological replicates. (**C**) Pre-confluent (day -4) BAT-LgT preadipocytes were transduced with lentivirus expressing either control luciferase shRNA (Control) or shRNA targeting KDM5A, KDM5B and KDM5C (KD). Cell counting at the indicated time points in the differentiation in control (blue) and KDM5 KD (red) BAT-LgT cells. Error bars represent SD ($n = 3$). (**D**) Quantification of Oil red O staining at day 7 of differentiation in BAT-LgT control (blue) and KDM5 KD (red) cells presented as Oil red O (ORO) signal per cell relative to control. (**E**) mRNA levels of uncoupling protein 1 (*Ucp1*) and adipocyte marker genes at day 6 in control (blue) and KDM5 KD (red) BAT-LgT cells. Error bars represent standard deviation (SD) ($n = 3$). *$P < 0.05$, **$P < 0.01$, and ***$P < 0.005$, Student's two-tailed *t*-test.

KDM5C, prevents masking of important functions of KDM5 demethylases due to redundancy and functional compensation between the subtypes. The fourth KDM5 family member, KDM5D, is not expressed in 3T3-L1 cells. The gene encoding KDM5D is found on the Y chromosome, which is present in 3T3-L1 preadipocytes but based on RNA-seq data appears to be completely silenced. We show that KD of KDM5 in 3T3-L1 preadipocytes leads to a large global increase in H3K4me3 promoter levels, thereby indicating that the KDM5 family is a major determinant of the level of H3K4me3 at promoters in these cells. Previous studies have assessed the effects of KD of individual KDM5 family members on H3K4me3 levels and arrived at different conclusions. Thus, in accordance with our observations, a global increase in H3K4me3 levels was reported in response to KDM5A KD in human gastric cancer cells (13), whereas no global changes were observed in KDM5A KO MEFs (7). Depletion of KDM5B resulted in a global increase in H3K4me3 levels in ESCs (23) and breast cancer cells (88) but not in neuronal stem cells (23). By contrast, KDM5B KD in MCF7 cells (17) and KDM5C KD in ESCs (38) only resulted in local site-specific effects on H3K4me3 levels. The differences in the results obtained are likely due to the redundancy between KDM5 family members and the different cellular contexts of the studies. High levels of H3K4me3 are generally associated with active promoters (1,29,33). Our finding that the increase in gene expression of a subset of genes correlates strongly with the increase in promoter H3K4me3 levels is consistent with that. However, the fact that the robust increase in the H3K4me3 mark at promoters upon KDM5 KD is not correlated with gene expression indicates that increased deposition of H3K4me3 is generally insufficient for activation of gene expression.

Members of the KDM5 family have been reported as both activators and repressors of gene transcription dependent on the cellular context (3,12–14,17,21–23,27,28,34–38,76,88). Interestingly, we show that high KDM5A binding appears to predispose promoters for early activation during 3T3-L1 differentiation and that KD of KDM5 leads to diminished activation of many of these genes, thereby suggesting a direct role of KDM5 in the transcriptional activation of this subset of target genes. Notably, KDM5-activated promoters typically have high KDM5A and KDM5C occupancy, and high levels of H3K4me3 and promoter activity, whereas KDM5-repressed promoters generally have low KDM5A and KDM5C occupancy and low levels of H3K4me3 and promoter activity. Thus, KDM5 appears to function as a repressor at some promoters, which are generally low occupancy sites, whereas it acts as an activator of a subset of high KDM5 occupancy promoters. In line with this, lysine-specific histone demethylase 1A (KDM1A/LSD1) was recently shown to exert a dual role at androgen-regulated enhancers, where LSD1 mediates the removal of the H3K4me2 mark, but still acts as a

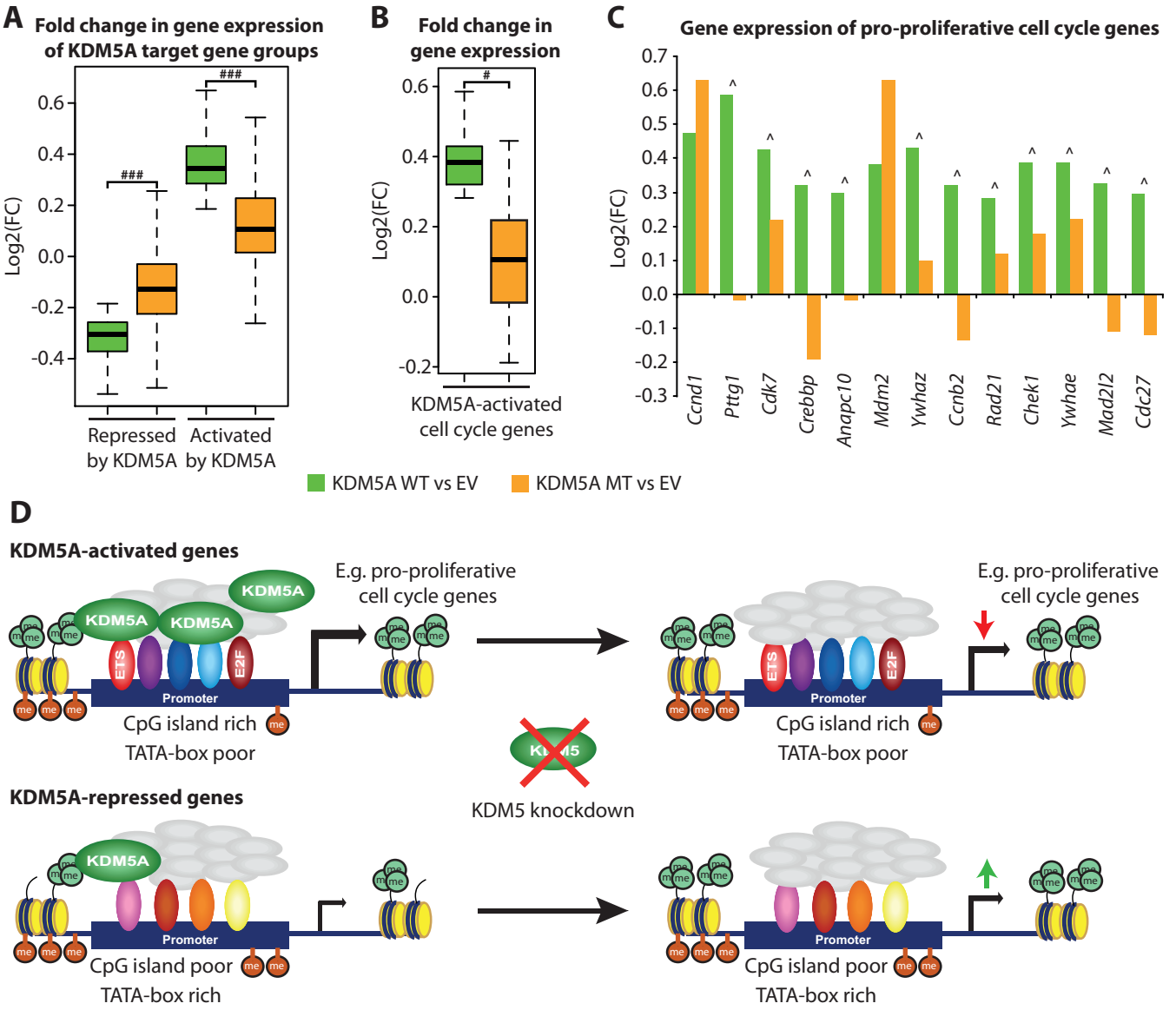

Figure 8. KDM5A enzymatic activity is required for KDM5A-mediated activation as well as repression of genes. (**A**) Log2 fold change in expression of genes either repressed (left) or activated (right) in KDM5A KO MEFs with ectopic expression of WT KDM5A compared to EV cells (green) or KDM5A KO MEFs with ectopic expression of MT KDM5A compared to EV cells (orange). Log2 fold change in expression of (**B**) all cell cycle genes; or (**C**) previously reported pro-proliferative cell cycle genes activated by reintroduction of KDM5A WT in KDM5A KO MEFs. Genes marked by '^' are significantly activated by reintroduction of KDM5A WT but not KDM5A MT (Padj<0.1). (A and B) *P*-value: # $P < 0.05$ and ### $P <$ 2.2e-16, Wilcoxon rank sum test. (**D**) Features of KDM5-regulated promoters. KDM5-activated promoters are generally CpG-island rich promoters that are depleted in CpG methylation and characterized by having high occupancy of KDM5A, high levels of H3K4me3, and their associated genes are highly expressed. When the KDM5s are knocked down, the expression of genes associated with KDM5-activated promoters decreases with minor effects on H3K4me3 promoter levels. KDM5-repressed promoters are generally rich in TATA-boxes and less depleted of CpG methylation, and they display low occupancy of KDM5A, low levels of H3K4me3, and low expression of the associated genes. Upon KD of KDM5, the expression of genes associated with KDM5-repressed promoters is increased with a concomitant considerable gain in H3K4me3 promoter signal.

coactivator probably through demethylation of other histone or non-histone substrates (89).

The molecular basis for this apparent dual role of the KDM5s in the regulation of promoter activity is unclear; however, it is possible that this is controlled by a promoter context-dependent balance between the coactivator function and the H3K4me3 demethylase activity. In this regard it is interesting that KDM5-activated promoters are generally devoid of a TATA box, but have a high prevalence of CpG islands. Furthermore, the E2F binding motif is highly enriched in the group of KDM5-actived promoters. Importantly, our data suggest that the ability of KDM5A to repress and activate gene transcription is dependent on its demethylase domain. The mechanisms leading to this dependency remain unknown, but may involve demethylation of associated transcription factors and cofactors.

Interestingly, we show that cell cycle genes are among the most highly enriched gene pathway in the group of KDM5-

activated target genes and that KD of the KDM5s leads to impairment of early stage 3T3-L1 adipogenesis including mitotic clonal expansion in response to the differentiation cocktail. Since mitotic clonal expansion is required for adipocyte differentiation of 3T3-L1 adipocytes, it is likely that KDM5 KD interferes with adipocyte differentiation at least in part by interfering with post confluent proliferative potential. Consistent with that, if the KDM5s are knocked down at day 2, i.e. after activation of the second wave of adipogenic transcription factors (including PPARγ and C/EBPα) and after the post-confluent mitoses, adipogenesis is not significantly inhibited. KDM5 KD in BAT-LgT cells, which is a SV40 large-T antigen-immortalized brown preadipocyte model, reduced both the ability of these cells to proliferate and to accumulate lipids in response differentiation inducers. Some previous studies have reported a similar pro-proliferative role of the KDM5s (12–14,17,18), whereas the KDM5s in other cellular systems have been reported to be anti-proliferative (21,22,34,90,91). The very different cellular contexts of the studies, including malignant cell models, are likely responsible for the different functions assigned to the KDM5s. Our data show that the KDM5s have pro-proliferative effects in fibroblasts and preadipocytes and indicate that this is mediated by directly promoting the activation of the pro-proliferative cell cycle gene promoters. This may also have important mechanistic implications in other biological systems, since the KDM5 family is known to promote tumor growth in different cancer settings.

In conclusion, we show that members of the KDM5 family are required for mitotic clonal expansion and differentiation of 3T3-L1 preadipocytes and for post-confluent mitoses and full differentiation of the brown preadipocyte cell line BAT-LgT into mature adipocytes. KDM5 plays a key role in modulating the level of H3K4me3 at promoters of 3T3-L1 preadipocytes, but changes in H3K4me3 have a limited effect *per se* on gene expression. Instead, during early stage adipogenesis, the KDM5s appear to act as direct dual coregulators that, depending on the context, activate some promoters while repressing others. Specifically, the KDM5s appear to be exerting their main action on adipogenesis as direct coactivators of a subset of promoters, including promoters driving pro-proliferative cell cycle genes. Future investigation should delineate the molecular basis for the apparent dual role of the KDM5s as corepressors and coactivators.

SUPPLEMENTARY DATA

Supplementary Data are available at NAR Online.

ACKNOWLEDGEMENTS

The authors thank Dr Patrick Seale, University of Pennsylvania for kindly providing the immortalized brown preadipocytes utilized for this study and D. William Kaelin, Dana-Farber Cancer Institute, Harvard Medical School for contributions to the microarray data. Furthermore, the authors thank members of the Mandrup laboratory for experimental support and fruitful discussions.

FUNDING

Danish Independent Research Council | Natural Science; Novo Nordisk Foundation; research grant from the Danish Diabetes Academy supported by the Novo Nordisk Foundation; grant from the VILLUM Foundation to the VILLUM Center for Bioanalytical Sciences at University of Southern Denmark; American Cancer Society Research Scholar Grant [RSG-13-384-01-DMC to Q.Y.]. Funding for open access charge: Danish Independent Research Council | Natural Science.
Conflict of interest statement. None declared.

REFERENCES

1. Dunham,I., Kundaje,A., Aldred,S.F., Collins,P.J., Davis,C.A., Doyle,F., Epstein,C.B., Frietze,S., Harrow,J., Kaul,R. *et al.* (2012) An integrated encyclopedia of DNA elements in the human genome. *Nature*, **489**, 57–74.
2. Dimitrova,E., Turberfield,A.H. and Klose,R.J. (2015) Histone demethylases in chromatin biology and beyond. *EMBO Rep.*, **16**, 1620–1639.
3. DiTacchio,L., Le,H.D., Vollmers,C., Hatori,M., Witcher,M., Secombe,J. and Panda,S. (2011) Histone lysine demethylase JARID1a activates CLOCK-BMAL1 and influences the circadian clock. *Science*, **333**, 1881–1885.
4. Liu,X. and Secombe,J. (2015) The histone demethylase KDM5 activates gene expression by recognizing chromatin context through Its PHD reader motif. *Cell Rep.*, **13**, 2219–2231.
5. Miller,S.A., Mohn,S.E. and Weinmann,A.S. (2010) Jmjd3 and UTX play a demethylase-independent role in chromatin remodeling to regulate t-box family member-dependent gene expression. *Mol. Cell*, **40**, 594–605.
6. Christensen,J., Agger,K., Cloos,P.A.C, Pasini,D., Rose,S., Sennels,L., Rappsilber,J., Hansen,K.H., Salcini,A.E. and Helin,K. (2007) RBP2 belongs to a family of demethylases, specific for tri-and dimethylated lysine 4 on histone 3. *Cell*, **128**, 1063–1076.
7. Klose,R.J., Yan,Q., Tothova,Z., Yamane,K., Erdjument-Bromage,H., Tempst,P., Gilliland,D.G., Zhang,Y. and Kaelin,W.G. (2007) The retinoblastoma binding protein RBP2 is an H3K4 demethylase. *Cell*, **128**, 889–900.
8. Qian,S., Wang,Y., Ma,H. and Zhang,L. (2015) Expansion and functional divergence of the JmjC gene family: significance of duplications in ancestral angiosperms and vertebrates. *Plant Physiol.*, **168**, 1321–1337.
9. Jangravi,Z., Tabar,M.S., Mirzaei,M., Parsamatin,P., Vakilian,H., Alikhani,M., Shabani,M., Haynes,P.A., Goodchild,A.K., Gourabi,H. *et al.* (2015) Two splice variants of y chromosome-located lysine-specific Demethylase 5D have distinct function in prostate cancer cell line (DU-145). *J. Proteome Res.*, **14**, 3492–3502.
10. Jensen,L.R., Amende,M., Gurok,U., Moser,B., Gimmel,V., Tzschach,A., Janecke,A.R., Tariverdian,G., Chelly,J., Fryns,J.-P. *et al.* (2005) Mutations in the JARID1C gene, which is involved in transcriptional regulation and chromatin remodeling, cause X-linked mental retardation. *Am. J. Hum. Genet.*, **76**, 227–236.
11. Cao,J., Liu,Z., Cheung,W.K.C., Zhao,M., Chen,S.Y., Chan,S., Booth,C.J., Nguyen,D.X. and Yan,Q. (2014) Histone demethylase RBP2 is critical for breast cancer progression and metastasis. *Cell Rep.*, **6**, 868–877.
12. Lin,W., Cao,J., Liu,J., Beshiri,M.L., Fujiwara,Y., Francis,J., Cherniack,A.D., Geisen,C., Blair,L.P., Zou,M.R. *et al.* (2011) Loss of the retinoblastoma binding protein 2 (RBP2) histone demethylase suppresses tumorigenesis in mice lacking Rb1 or Men1. *Proc. Natl. Acad. Sci. U.S.A.*, **108**, 13379–13386.
13. Zeng,J., Ge,Z., Wang,L., Li,Q., Wang,N., Björkholm,M., Jia,J. and Xu,D. (2010) The histone demethylase RBP2 Is overexpressed in gastric cancer and its inhibition triggers senescence of cancer cells. *Gastroenterology*, **138**, 981–992.
14. Teng,Y.-C., Lee,C.-F., Li,Y.-S., Chen,Y.-R., Hsiao,P.-W., Chan,M.-Y., Lin,F.-M., Huang,H.-D., Chen,Y.-T., Jeng,Y.-M. *et al.* (2013) Histone demethylase RBP2 promotes lung tumorigenesis and cancer metastasis. *Cancer Res.*, **73**, 4711–4721.

15. Lu,P.J., Sundquist,K., Baeckstrom,D., Poulsom,R., Hanby,A, Meier-Ewert,S., Jones,T., Mitchell,M., Pitha-Rowe,P., Freemont,P. *et al.* (1999) A novel gene (PLU-1) containing highly conserved putative DNA/chromatin binding motifs is specifically up-regulated in breast cancer. *J. Biol. Chem.*, **274**, 15633–15645.
16. Barrett,A., Madsen,B., Copier,J., Lu,P.J., Cooper,L., Scibetta,A.G., Burchell,J. and Taylor-Papadimitriou,J. (2002) PLU-1 nuclear protein, which is upregulated in breast cancer, shows restricted expression in normal human adult tissues: a new cancer/testis antigen? *Int. J. Cancer*, **101**, 581–588.
17. Yamane,K., Tateishi,K., Klose,R.J., Fang,J., Fabrizio,L.A., Erdjument-Bromage,H., Taylor-Papadimitriou,J., Tempst,P. and Zhang,Y. (2007) PLU-1 is an H3K4 demethylase involved in transcriptional repression and breast cancer cell proliferation. *Mol. Cell*, **25**, 801–812.
18. Scibetta,A.G., Santangelo,S., Coleman,J., Hall,D., Chaplin,T., Copier,J., Catchpole,S., Burchell,J. and Taylor-Papadimitriou,J. (2007) Functional analysis of the transcription repressor PLU-1/JARID1B. *Mol. Cell. Biol.*, **27**, 7220–7235.
19. Stein,J., Majores,M., Rohde,M., Lim,S., Schneider,S., Krappe,E., Ellinger,J., Dietel,M., Stephan,C., Jung,K. *et al.* (2014) KDM5C is overexpressed in prostate cancer and is a prognostic marker for prostate-specific antigen-relapse following radical prostatectomy. *Am. J. Pathol.*, **184**, 2430–2437.
20. Dalgliesh,G.L., Furge,K., Greenman,C., Chen,L., Bignell,G., Butler,A., Davies,H., Edkins,S., Hardy,C., Latimer,C. *et al.* (2010) Systematic sequencing of renal carcinoma reveals inactivation of histone modifying genes. *Nature*, **463**, 360–363.
21. Lopez-Bigas,N., Kisiel,T.A., Dewaal,D.C., Holmes,K.B., Volkert,T.L., Gupta,S., Love,J., Murray,H.L., Young,R.A. and Benevolenskaya,E. V. (2008) Genome-wide analysis of the H3K4 histone demethylase RBP2 reveals a transcriptional program controlling differentiation. *Mol. Cell*, **31**, 520–530.
22. Beshiri,M.L., Holmes,K.B., Richter,W.F., Hess,S., Islam,A.B.M.M.K., Yan,Q., Plante,L., Litovchick,L., Gévry,N., Lopez-Bigas,N. *et al.* (2012) Coordinated repression of cell cycle genes by KDM5A and E2F4 during differentiation. *Proc. Natl. Acad. Sci. U.S.A.*, **109**, 18499–18504.
23. Schmitz,S.U., Albert,M., Malatesta,M., Morey,L., Johansen,J. V., Bak,M., Tommerup,N., Abarrategui,I. and Helin,K. (2011) Jarid1b targets genes regulating development and is involved in neural differentiation. *EMBO J.*, **30**, 4586–4600.
24. Kaufmann,K., Van Ijcken,W.F.J., Koerkamp,M.J.G., Outchkourov,N.S., Muin,J.M., Van Leenen,D., De Graaf,P., Holstege,F.C.P., Grosveld,F.G. and Timmers,H.T.M. (2013) Balancing of Histone H3K4 Methylation States by the Kdm5c/SMCX Histone Demethylase Modulates Promoter and Enhancer Function. *Cell Rep.*, **3**, 1071–1079.
25. Lee,M.G., Norman,J., Shilatifard,A. and Shiekhattar,R. (2007) Physical and functional association of a trimethyl H3K4 demethylase and Ring6a/MBLR, a polycomb-like protein. *Cell*, **128**, 877–887.
26. Shen,H., Xu,W., Guo,R., Shen,H., Xu,W., Guo,R., Rong,B., Gu,L., Wang,Z., He,C. *et al.* (2016) Suppression of enhancer overactivation by a RACK7-histone demethylase complex. *Cell*, **165**, 331–342.
27. Xie,L., Pelz,C., Wang,W., Bashar,A., Varlamova,O., Shadle,S. and Impey,S. (2011) KDM5B regulates embryonic stem cell self-renewal and represses cryptic intragenic transcription. *EMBO J.*, **30**, 1473–1484.
28. Kidder,B.L., Hu,G. and Zhao,K. (2014) KDM5B focuses H3K4 methylation near promoters and enhancers during embryonic stem cell self-renewal and differentiation. *Genome Biol.*, **15**.
29. Heintzman,N.D., Stuart,R.K., Hon,G., Fu,Y., Ching,C.W., Hawkins,R.D., Barrera,L.O., Van Calcar,S., Qu,C., Ching,K. A. *et al.* (2007) Distinct and predictive chromatin signatures of transcriptional promoters and enhancers in the human genome. *Nat. Genet.*, **39**, 311–318.
30. Roh,T.-Y., Cuddapah,S., Cui,K. and Zhao,K. (2006) The genomic landscape of histone modifications in human T cells. *Proc. Natl. Acad. Sci. U.S.A.*, **103**, 15782–15787.
31. Pekowska,A., Benoukraf,T., Ferrier,P. and Spicuglia,S. (2010) A unique H3K4me2 profile marks tissue-specific gene regulation. *Genome Res.*, **20**, 1493–1502.
32. Siersbæk,R., Rabiee,A., Nielsen,R., Sidoli,S., Traynor,S., Loft,A., Poulsen,L., Rogowska-Wrzesinska,A., Jensen,O.N. and Mandrup,S. (2014) Transcription factor cooperativity in early adipogenic hotspots and super-enhancers. *Cell Rep.*, **7**, 1443–1455.
33. Santos-Rosa,H., Schneider,R., Bannister,A.J., Sherriff,J., Bernstein,B.E., Emre,N.C.T., Schreiber,S.L., Mellor,J. and Kouzarides,T. (2002) Active genes are tri-methylated at K4 of histone H3. *Nature*, **419**, 407–411.
34. Chicas,A., Kapoor,A., Wang,X., Aksoy,O., Evertts,A.G., Zhang,M.Q., Garcia,B. A., Bernstein,E. and Lowe,S.W. (2012) H3K4 demethylation by Jarid1a and Jarid1b contributes to retinoblastoma-mediated gene silencing during cellular senescence. *Proc. Natl. Acad. Sci. U.S.A.*, **109**, 8971–8976.
35. Váraljai,R., Islam,A.B.M.M.K., Beshiri,M.L., Rehman,J., Lopez-Bigas,N. and Benevolenskaya,E. V (2015) Increased mitochondrial function downstream from KDM5A histone demethylase rescues differentiation in pRB-deficient cells. *Genes Dev.*, **29**, 1817–1834.
36. Benevolenskaya,E. V, Murray,H.L., Branton,P., Young,R. A. and Kaelin,W.G. (2005) Binding of pRB to the PHD protein RBP2 promotes cellular differentiation. *Mol. Cell*, **18**, 623–635.
37. Chan,S.W. and Hong,W. (2001) Retinoblastoma-binding protein 2 (Rbp2) potentiates nuclear hormone receptor-mediated transcription. *J. Biol. Chem.*, **276**, 28402–28412.
38. Outchkourov,N.S., Muiño,J.M., Kaufmann,K., van Ijcken,W.F.J., Groot Koerkamp,M.J., van Leenen,D., de Graaf,P., Holstege,F.C.P., Grosveld,F.G. and Timmers,H.T.M. (2013) Balancing of histone H3K4 methylation states by the Kdm5c/SMCX histone demethylase modulates promoter and enhancer function. *Cell Rep.*, **3**, 1071–1079.
39. Secombe,J., Li,L., Carlos,L. and Eisenman,R.N. (2007) The Trithorax group protein Lid is a trimethyl histone H3K4 demethylase required for dMyc-induced cell growth. *Genes Dev.*, **21**, 537–551.
40. Lee,N., Erdjument-Bromage,H., Tempst,P., Jones,R.S. and Zhang,Y. (2009) The H3K4 demethylase lid associates with and inhibits histone deacetylase Rpd3. *Mol. Cell. Biol.*, **29**, 1401–1410.
41. Liu,X., Greer,C. and Secombe,J. (2014) KDM5 Interacts with Foxo to Modulate Cellular Levels of Oxidative Stress. *PLoS Genet.*, **10**.
42. Cristancho,A.G. and Lazar,M.A. (2011) Forming functional fat: a growing understanding of adipocyte differentiation. *Nat. Rev. Mol. Cell Biol.*, **12**, 722–734.
43. Siersbæk,R., Nielsen,R. and Mandrup,S. (2012) Transcriptional networks and chromatin remodeling controlling adipogenesis. *Trends Endocrinol. Metab.*, **23**, 56–64.
44. Tang,Q.-Q., Otto,T.C. and Lane,M.D. (2003) CCAAT/enhancer-binding protein beta is required for mitotic clonal expansion during adipogenesis. *Proc. Natl. Acad. Sci. U.S.A.*, **100**, 850–855.
45. Yeh,W.C., Bierer,B.E. and McKnight,S.L. (1995) Rapamycin inhibits clonal expansion and adipogenic differentiation of 3T3-L1 cells. *Proc. Natl. Acad. Sci. U.S.A.*, **92**, 11086–11090.
46. Tang,Q.-Q., Otto,T.C. and Lane,M.D. (2003) Mitotic clonal expansion: a synchronous process required for adipogenesis. *Proc. Natl. Acad. Sci. U. S. A.*, **100**, 44–49.
47. Zhang,J.-W., Tang,Q.-Q., Vinson,C. and Lane,M.D. (2004) Dominant-negative C/EBP disrupts mitotic clonal expansion and differentiation of 3T3-L1 preadipocytes. *Proc. Natl. Acad. Sci. U.S.A.*, **101**, 43–47.
48. Mikkelsen,T.S., Xu,Z., Zhang,X., Wang,L., Gimble,J.M., Lander,E.S. and Rosen,E.D. (2010) Comparative epigenomic analysis of murine and human adipogenesis. *Cell*, **143**, 156–169.
49. Musri,M.M., Gomis,R. and Párrizas,M. (2010) A chromatin perspective of adipogenesis. *Organogenesis*, **6**, 15–23.
50. Steger,D.J., Grant,G.R., Schupp,M., Tomaru,T., Lefterova,M.I., Schug,J., Manduchi,E., Stoeckert,C.J. and Lazar,M. A (2010) Propagation of adipogenic signals through an epigenomic transition state. *Genes Dev.*, **24**, 1035–1044.
51. Musri,M.M. and Párrizas,M. (2012) Epigenetic regulation of adipogenesis. *Curr. Opin. Clin. Nutr. Metab. Care*, **15**, 342–349.
52. Ge,K. (2012) Epigenetic Regulation of Adipogenesis by Histone Methylation. *Biochem. Biophys. Acta*, **1819**, 727–732.
53. Helledie,T., Grøntved,L., Jensen,S.S., Kiilerich,P., Rietveld,L., Albrektsen,T., Boysen,M.S., Nøhr,J., Larsen,L.K., Fleckner,J. *et al.* (2002) The gene encoding the acyl-CoA-binding protein is activated by peroxisome proliferator-activated receptor γ through an intronic response element functionally conserved between humans and rodents. *J. Biol. Chem.*, **277**, 26821–26830.

54. Nielsen,R., Grøntved,L., Stunnenberg,H.G. and Mandrup,S. (2006) Peroxisome proliferator-activated receptor subtype- and cell-type-specific activation of genomic target genes upon adenoviral transgene delivery. *Mol. Cell. Biol.*, **26**, 5698–5714.
55. Ventura,A., Meissner,A., Dillon,C.P., McManus,M., Sharp,P. A., Van Parijs,L., Jaenisch,R. and Jacks,T. (2004) Cre-lox-regulated conditional RNA interference from transgenes. *Proc. Natl. Acad. Sci. U.S.A.*, **101**, 10380–10385.
56. Siersbæk,M.S., Loft,A., Aagaard,M.M., Nielsen,R., Schmidt,S.F., Petrovic,N., Nedergaard,J. and Mandrup,S. (2012) Genome-wide profiling of peroxisome proliferator-activated receptor gamma in primary epididymal, inguinal, and brown adipocytes reveals depot-selective binding correlated with gene expression. *Mol. Cell. Biol.*, **32**, 3452–3463.
57. Loft,A., Forss,I., Siersbæk,M.S., Schmidt,S.F., Larsen,A.B., Madsen,J.G.S., Pisani,D.F., Nielsen,R., Aagaard,M.M., Mathison,A. *et al.* (2015) Browning of human adipocytes requires KLF11 and reprogramming of PPARγ superenhancers. *Genes Dev.*, **29**, 7–22.
58. Nielsen,R. and Mandrup,S. (2014) Genome-Wide Profiling of Transcription Factor Binding and Epigenetic Marks in Adipocytes by ChIP-seq. *Methods Enzymol.*, **537**, 261-279.
59. Smyth,G.K. (2004) Linear models and empirical Bayes methods for assessing differential expression in microarray experiments. *Stat. Appl. Genet. Mol. Biol.*, **3**, 1–26.
60. Langmead,B. and Salzberg,S.L. (2012) Fast gapped-read alignment with Bowtie 2. *Nat. Methods*, **9**, 357–359.
61. Habegger,L., Sboner,A., Gianoulis,T.A., Rozowsky,J., Agarwal,A., Snyder,M. and Gerstein,M. (2011) RSEQtools: a modular framework to analyze RNA-Seq data using compact, anonymized data summaries. *Bioinformatics*, **27**, 281–283.
62. Liao,Y., Smyth,G.K. and Shi,W. (2013) The Subread aligner: Fast, accurate and scalable read mapping by seed-and-vote. *Nucleic Acids Res.*, **41**, 1–17.
63. Love,M.I., Huber,W. and Anders,S. (2014) Moderated estimation of fold change and dispersion for RNA-seq data with DESeq2. *Genome Biol.*, **15**, 550.
64. Kumar,L. and Futschik,M. (2007) Mfuzz: A software package for soft clustering of microarray data. *Bioinformation*, **2**, 5–7.
65. Heinz,S., Benner,C., Spann,N., Bertolino,E., Lin,Y.C., Laslo,P., Cheng,J.X., Murre,C., Singh,H. and Glass,C.K. (2010) Simple combinations of lineage-determining transcription factors prime cis-regulatory elements required for macrophage and B cell identities. *Mol. Cell*, **38**, 576–589.
66. Kanehisa,M. and Goto,S. (2000) KEGG: Kyoto Encyclopaedia of Genes and Genomes. *Nucleic Acids Res.*, **28**, 27–30.
67. Kanehisa,M., Goto,S., Sato,Y., Kawashima,M., Furumichi,M. and Tanabe,M. (2014) Data, information, knowledge and principle: back to metabolism in KEGG. *Nucleic Acids Res.*, **42**, D199–D205.
68. Kutmon,M., Riutta,A., Nunes,N., Hanspers,K., Willighagen,E.L., Bohler,A., Mélius,J., Waagmeester,A., Sinha,S.R., Miller,R. *et al.* (2015) WikiPathways: capturing the full diversity of pathway knowledge. *Nucleic Acids Res.*, **44**, D488–D494.
69. Dobin,A., Davis,C.A., Schlesinger,F., Drenkow,J., Zaleski,C., Jha,S., Batut,P., Chaisson,M. and Gingeras,T.R. (2013) STAR: ultrafast universal RNA-seq aligner. *Bioinformatics*, **29**, 15–21.
70. Lun,A.T.L. and Smyth,G.K. (2014) De novo detection of differentially bound regions for ChIP-seq data using peaks and windows: Controlling error rates correctly. *Nucleic Acids Res.***42**, 1–11.
71. Kent,W.J., Sugnet,C.W., Furey,T.S., Roskin,K.M., Pringle,T.H., Zahler,A.M. and Haussler,D. (2002) The Human Genome Browser at UCSC The Human Genome Browser at UCSC. *Genome Res.*, **12**, 996–1006.
72. Dreos,R., Ambrosini,G., Cavin Perier,R. and Bucher,P. (2013) EPD and EPDnew, high-quality promoter resources in the next-generation sequencing era. *Nucleic Acids Res.*, **41**, D157–D164.
73. Saxonov,S., Berg,P. and Brutlag,D.L. (2006) A genome-wide analysis of CpG dinucleotides in the human genome distinguishes two distinct classes of promoters. *Proc. Natl. Acad. Sci. U.S.A.*, **103**, 1412–1417.
74. Matsumura,Y., Nakaki,R., Inagaki,T., Yoshida,A., Kano,Y., Kimura,H., Tanaka,T., Tsutsumi,S., Nakao,M., Doi,T. *et al.* (2015) H3K4/H3K9me3 bivalent chromatin domains targeted by lineage-specific DNA methylation pauses adipocyte differentiation. *Mol. Cell*, **60**, 584–596.
75. Siersbæk,R. and Mandrup,S. (2011) Transcriptional networks controlling adipocyte differentiation. *Cold Spring Harb. Symp. Quant. Biol.*, **76**, 247–255.
76. Pasini,D., Hansen,K.H., Christensen,J., Agger,K., Cloos,P. A. C. and Helin,K. (2008) Coordinated regulation of transcriptional repression by the RBP2 H3K4 demethylase and Polycomb-Repressive Complex 2. *Genes Dev.*, **22**, 1345–1355.
77. Huang,S.Q., Liao,Q.J., Wang,X.W., Xin,D.Q., Chen,S.X., Wu,Q.J., Ye,G., Huang,S.Q., Liao,Q.J., Wang,X.W. *et al.* (2012) RNAi-mediated knockdown of pituitary tumor-transforming gene-1 (PTTG1) suppresses the proliferation and invasive potential of PC3 human prostate cancer cells RNAi-mediated knockdown of pituitary tumor- transforming gene-1 (PTTG1) suppresses the prolif. *Brazilian J. Med. Biol. Res.*, **45**, 995–1001.
78. Caporali,S., Alvino,E., Levati,L., Esposito,A.I., Ciomei,M., Brasca,M.G., Del,D., Desideri,M., Bonmassar,E., Pfeffer,U. *et al.* (2012) Down-regulation of the PTTG1 proto-oncogene contributes to the melanoma suppressive effects of the cyclin-dependent kinase inhibitor PHA-848125. *Biochem. Pharmacol.*, **84**, 598–611.
79. Ganuza,M., Sa,C., Go,G., Schneider,R., Blasco,A. and Pisano,D. (2012) Genetic inactivation of Cdk7 leads to cell cycle arrest and induces premature aging due to adult stem cell exhaustion. *EMBO J.*, **31**, 2498–2510.
80. Atienza,J.M., Roth,R.B., Rosette,C., Smylie,K.J., Kammerer,S., Rehbock,J., Ekblom,J. and Denissenko,M.F. (2005) Suppression of RAD21 gene expression decreases cell growth and enhances cytotoxicity of etoposide and bleomycin in human breast cancer cells. *Mol. Cancer Ther.*, **4**, 361–368.
81. Shubbar,E., Kovács,A., Hajizadeh,S., Parris,T.Z., Nemes,S., Gunnarsdóttir,K., Einbeigi,Z., Karlsson,P. and Helou,K. (2013) Elevated cyclin B2 expression in invasive breast carcinoma is associated with unfavorable clinical outcome. *BMC Cancer*, **13**, doi:10.1186/1471-2407-13-1.
82. Khanna,A., Kauko,O., Böckelman,C., Laine,A., Schreck,I., Partanen,J.I., Szwajda,A., Bormann,S., Bilgen,T., Helenius,M. *et al.* (2013) Chk1 Targeting Reactivates PP2A Tumor Suppressor Activity in Cancer Cells. *Cancer Res.*, **73**, 6757–6769.
83. Nishimura,Y., Komatsu,S., Ichikawa,D., Nagata,H., Hirajima,S., Takeshita,H., Kawaguchi,T., Arita,T., Konishi,H., Kashimoto,K. *et al.* (2013) Overexpression of YWHAZ relates to tumor cell proliferation and malignant outcome of gastric carcinoma. *Br. J. Cancer*, **108**, 1324–1331.
84. Qiu,L., Wu,J., Pan,C., Tan,X., Lin,J., Liu,R., Chen,S., Geng,R. and Huang,W. (2016) Downregulation of CDC27 inhibits the proliferation of colorectal cancer cells via the accumulation of p21Cip1/Waf1. *Cell Death Dis.*, **7**, e2074.
85. Rimkus,C., Friederichs,J., Rosenberg,R., Holzmann,B., Siewert,J.-R. and Janssen,K. (2006) Expression of the mitotic checkpoint gene MAD2L2 has prognostic significance in colon cancer. *Int. J. Cancer*, **120**, 207–211.
86. Raungrut,P., Wongkotsila,A., Lirdprapamongkol,K., Svasti,J., Geater,S.L., Phukaoloun,M., Suwiwat,S. and Thongsuksai,P. (2014) Prognostic significance of 14-3-3-3γ overexpression in advanced non-small cell lung cancer. *Asian Pacific J. Cancer Prev.*, **15**, 3513–3518.
87. Haines,D.S. (1997) The mdm2 Proto-Oncogene. *Leuk. Lymphoma*, **26**, 227–238.
88. Klein,B.J., Piao,L., Xi,Y., Rincon-Arano,H., Rothbart,S.B., Peng,D., Wen,H., Larson,C., Zhang,X., Zheng,X. *et al.* (2014) The Histone-H3K4-Specific Demethylase KDM5B Binds to Its Substrate and Product through Distinct PHD Fingers. *Cell Rep.*, **6**, 325–335.
89. Cai,C., He,H.H., Gao,S., Chen,S., Yu,Z., Gao,Y., Chen,S., Chen,M.W., Zhang,J., Ahmed,M. *et al.* (2014) Lysine-specific demethylase 1 has dual functions as a major regulator of androgen receptor transcriptional activity. *Cell Rep.*, **9**, 1618–1627.
90. Gutierrez,G.M., Kong,E. and Hinds,P.W. (2005) Master or slave: the complex relationship of RBP2 and pRb. *Cancer Cell*, **7**, 501–502.
91. Roesch,A., Mueller,A.M., Stempfl,T., Moehle,C., Landthaler,M. and Vogt,T. (2008) RBP2-H1/JARID1B is a transcriptional regulator with a tumor suppressive potential in melanoma cells. *Int. J. Cancer*, **122**, 1047–1057.